https://doi.org/10.5194/acp-2019-1012
Preprint. Discussion started: 16 December 2019

Atmospheric Chemistry and Physics Discussions

The role of HONO in O_3 formation and insight into its formation mechanism during the KORUS-AQ Campaign

Junsu Gil[1)], Jeonghwan Kim[2)], Meehye Lee[1)], Gangwoong Lee[2)], Dongsoo Lee[3)], Jinsang Jung[4)], Joonyeong An[5)], Jinkyu Hong[6)], Seogju Cho[7)], Jeonghoon Lee[8)], Russell Long[9)]

[1] *Department of Earth and Environmental Sciecne, Korea University, Seoul, Korea*
[2] *Department of Environmental Sciecne, Hankuk University of Foreign Studies, Yongin, Korea*
[3] *Department of Chemistry, Yonsei University, Seoul, Korea*
[4] *Korea Research Institute of Standards and Science (KRISS), Daejeon, Korea*
[5] *National Institute of Environmental Research (NIER), Incheon, Korea*
[6] *Department of Atmospheric Sciences, Yonsei University, Seoul, Korea*
[7] *Seoul Research Institute of Public Health and Environment, Seoul, Korea*
[8] *School of Mechanical Engineering, Korea University of Technology and Education, Cheonan, Korea*
[9] *United States Environmental Protection Agency, Washington, USA*

* *Correspondence to*: Meehye Lee (meehye@korea.ac.kr)

https://doi.org/10.5194/acp-2019-1012
Preprint. Discussion started: 16 December 2019

Atmospheric Chemistry and Physics Discussions

ABSTRACT

Photolysis of nitrous acid (HONO) has long been recognized as an early morning source of OH radicals in urban air, but the detailed mechanism of its formation is still unclear. During the Korea-US Air Quality (KORUS-AQ) campaign, HONO was measured using Quantum Cascade Tunable Diode Laser Absorption Spectroscopy (QC-TDLAS) at Olympic Park in Seoul from 17 May to 10 June, 2016. HONO concentrations ranged from 0.07 ppbv to 3.46 ppbv with an average of 0.93 ppbv. HONO remained high at night from 1 am to 5 am, during which the mean concentration was higher in high-O_3 episodes (1.82 ppbv) than non-episode (1.20 ppbv). In the morning, OH budget due to HONO photolysis were higher by 50 % (0.95 pptv) during high-O_3 episodes compared to non-episode. Diurnal variations of HO_x and O_3 simulated by the F0AM model demonstrated a difference of ~20 ppbv in daily maximum O_3 between the two periods. The HONO concentration increased with relative humidity (RH) until 80 %, of which the highest HONO was associated with the top 10 % NO_x, confirming that NO_x is a crucial precursor of HONO and its formation is facilitated by humidity. The conversion ratio of NO_x to HONO was estimated to be 0.86×10^{-2} h^{-1} at night and also increased with RH. As surrogate for the catalyst surface, the mass concentrations of black carbon (eBC) and the surface areas of particles smaller than 120 nm showed a tendency for RH similar to conversion ratio. Using an Artificial Neuron Network (ANN) model, HONO concentrations were successfully simulated with measured variables ($r = 0.8$ for the best suite), among which NO_x, surface area, and RH were found to be main factors affecting ambient HONO concentrations with weigh values of 26.2 %, 11.9 %, and 10.6 %, respectively. This study demonstrates the coupling of HONO with HO_x-VOCs-O_3 cycle in Seoul Metropolitan Areas (SMA) and provides practical evidence for heterogeneous formation of HONO by employing the ANN model to atmospheric chemistry.

https://doi.org/10.5194/acp-2019-1012
Preprint. Discussion started: 16 December 2019

Atmospheric Chemistry and Physics Discussions

1 INTRODUCTION

The photolysis of nitrous acid (HONO) can severely impact the OH budget in the lower atmosphere (Brandenburger et al., 1998;Plass-Dülmer et al., 1998;Kotamarthi et al., 2001;Xing et al., 2019) through the following reaction.

$$HONO + h\nu \rightarrow NO + OH \ (300nm < \lambda < 405\ nm) \qquad (R1)$$

In recent studies, R1 was shown to contribute daily OH formation up to 30 %, and strongly impacted the early morning OH budget, which finally caused the oxidation capacity to increase, even in low HONO concentrations (Alicke et al., 2002;Ryan et al., 2018). HONO accelerates the morning oxidation process by transferring OH through the HONO-VOCs-O_3 chain and provides NO_x (Alicke et al., 2003).This implies that there is a huge influence of HONO on the early morning photochemistry cycle, along with the promotion of VOC oxidation, causing high O_3 concentrations in afternoon (Aumont et al., 2003;Alicke et al., 2003;Kleffmann, 2007). Therefore, it is important to observe and predict the atmospheric HONO in order to understand the HO_x (HO_2 + OH) and NO_x (NO + NO_2) chemistry which influences O_3 production (Pitts and Pitts, 2000).

Although the importance of HONO to O_3 production was suggested in previous research, its role has not been fully understood due to the intricacies involved in HONO and O_3 formation under variety of ambient conditions. Recently, the high O_3 mechanism was a major concern in lots of studies. The Korea US – Air Quality (KORUS-AQ) campaign is one of these researches which made efforts to solve the photochemical pollution problem. KORUS-AQ campaign was conducted in May to June 2016, at Seoul Metropolitan Area (SMA) in South Korea. SMA is one of the most populated regions in the world, and it has been reported that SMA suffers from poor air quality caused by high concentrations of O_3 and $PM_{2.5}$ (Kim et al., 2018a;Kim et al., 2018b). In SMA, a better understanding of the chemical mechanisms is needed due to high NO_x-levels and dynamic change in meteorology which further complicates the photochemical process (Park, 2018;Kim et al., 2016;Ryu et al., 2013). During the KORUS-AQ campaign, airborne, satellite, and ground level measurements were conducted simultaneously within the same space-time frame. This provided a good opportunity for a comprehensive study of the chemical processes at high-NO_x condition and overall insight into the photochemical cycle, encompassing gaseous and particle phase.

To measure the HONO, a number of techniques have been adopted. Annular Denuder (AD) coupled with Ion Chromatography (IC) was commonly used in the beginning (Ferm and Sjödin, 1985;Allegrini et al., 1987;Koutrakis et al., 1988;Appel et al., 1990;Komazaki et al., 1999). This collection system has been improved to Diffusion Denuder (DD) and Parallel Plate Diffusion Scrubber (PPDS), lowing detection limit to several ppt levels with less interference from other nitrogen species (Keuken et al., 1988;Simon et al., 1991;Simon and Dasgupta, 1993, 1995). This configuration has been utilized to date without any major changes (Takeuchi et al., 2004;Li et al., 2017c;Gu et al., 2009;Song et al., 2009;Kim et al., 2015). A Measuring AeRosols and GAses (MARGA) system is similar to PPDS-IC instruments at the point of measuring water-soluble trace gases as ionic species using a denuder. It can detect low concentrations and has shown clear variation, as have other comparison methods; however, it has been required to show improved accuracy until recently due to its artifacts (Makkonen et al., 2012;Stieger et al., 2018).

The introduction of spectroscopy technique has facilitated HONO measurement through instrumentation such as Chemical Ionization Mass Spectrometry (CIMS) (Fortner et al., 2004;Roberts et al., 2010;Levy et al., 2014), Cavity

https://doi.org/10.5194/acp-2019-1012
Preprint. Discussion started: 16 December 2019

Atmospheric Chemistry and Physics Discussions

Ring Down Spectrometry (CRDS) (O'Keefe and Deacon, 1988;Scherer et al., 1997;Wheeler et al., 1998), Differential Optical Absorption Spectrometry (DOAS) (Winer and Biermann, 1994;Febo et al., 1996;Hendrick et al., 2014;Kleffmann et al., 2006;Stutz et al., 2010;Garcia-Nieto et al., 2018;Perner and Platt, 1979), and Photo Fragmentation with Laser Induced Fluorescence (PF-LIF) (Liao et al., 2006). All these methods have their own advantages and limitation. For example, CRDS has the advantage of short time resolution, but has a relatively high detection limit (Wang and Zhang, 2000). PF-LIF has the strength to measure low concentrations and has a short time resolution, but shows high uncertainty compared with other methods. Recently, Long Path Absorption Photometer (LOPAP) that is specialized to detecting high HONO concentrations, has been employed for field measurements and chamber studies (Heland et al., 2001;Kleffmann et al., 2006;Rohrer et al., 2005).

In addition, improved open-path spectroscopy, using Quantum Cascade Tunable Diode Laser Absorption Spectroscopy (QC-TDLAS) has been applied in HONO measurements (Lee et al., 2011;Cui et al., 2018b). It is more stable at room temperature without cooling, and easy to calibrate compared with using normal diode lasers. The inter-comparison study of HONO instruments conducted in polluted condition demonstrated that there was general agreement among all techniques and of these, TIDLAS instrument was used as a basis for pairwise comparison (Pinto et al., 2014).

The HONO formation mechanism is still not fully elucidated, albeit the progress in HONO measurement techniques. There have been several suggestions for HONO formation reactions during the nighttime, but most models have failed to accurately simulate HONO concentrations because various homogeneous and heterogeneous reactions are involved in the production of HONO under certain conditions (Su et al., 2011;Sun et al., 2001;Aumont et al., 2003;Kim et al., 2015;Su et al., 2008;Fu et al., 2019;Zhang et al., 2019a).

$NO + OH \rightarrow HONO$ (R2)

$NO_2 + H_2O \rightarrow HONO + OH$ (R3)

NO_2 + *ortho,para*-nitrophenols → HONO (R4)

$2NO_2 + H_2O + NH_3 \rightarrow HONO + NH_4NO_3$ (R5)

$2NO_2 + H_2O \rightarrow HONO + HNO_3$ (R6)

$NO_2 + NO + H_2O \rightarrow 2HONO$ (R7)

$NO + HNO_3 \rightarrow HONO + NO_2$ (R8)

NO_2 + *Soot* → HONO (R9)

NO_2 + VOCs → HONO (R10)

The reaction (R2) is well known as a HONO source in high NO and OH environments. This homogeneous reaction is a major process for HONO production, but it is not sufficient to explain the HONO concentration in low OH environments, especially during the nighttime (Kurtenbach et al., 2001). Therefore, other reactions (R3, R4, R5) were suggested (Bejan et al., 2006;Li et al., 2008;Zhang and Tao, 2010;Barsotti et al., 2017), but the estimated HONO budget still shows great uncertainty (Liu et al., 2019a). As a result, several studies suggested the possibility of HONO being formed by heterogeneous reactions occurring on surfaces. Several laboratory and outdoor studies considered aqueous and dry surfaces as reaction catalysts (Bari et al., 2003;Finlayson-Pitts et al., 2003;Wang et al., 2017;Spataro et al., 2017), including aerosol (Hendrick et al., 2014;Tong et al., 2016;Bernard et al., 2016;Wang et al., 2016;Lu et al., 2018), black carbon (Liang et al., 2017), and humic acid (Han et al., 2017;Yang et al., 2018) (R6~R10). Moreover, the surface includes

https://doi.org/10.5194/acp-2019-1012
Preprint. Discussion started: 16 December 2019

Atmospheric Chemistry and Physics Discussions

not only atmospheric particles but also ground soils, with the report of direct soil emission (Meusel et al., 2018;Bhattarai et al., 2018). These heterogeneous conversions and emissions from soil are controlled by several conditions such as pH, moisture, and microbials and mainly affect daytime HONO concentrations (Ermel et al., 2018;Wu et al., 2019). For these reactions, the measurement of active surface area hinders the accurate estimation of HONO formation (Romer et al., 2016). Recently, the photochemical reaction involving a nitrate series (HNO_3, NO_3^-) was considered as a major daytime HONO source (Han et al., 2017;Li et al., 2018;Ye et al., 2017;Tsai et al., 2018;Cui et al., 2019). The HONO production reaction is still controversial due to a wide variety of environments involving NO_x, RH, and surfaces and incomplete understanding of multi-phase reaction (Bao et al., 2018;Zhang et al., 2019c;Wen et al., 2019;Zhang et al., 2019b). In this context, new approaches are needed to elucidate the HONO formation mechanism.

In this study, we conducted a measurement and modeling at Olympic Park in Seoul for two purposes: To figure out the photochemical processes responsible for high O_3, with an emphasis on HONO that contributes the early morning OH budget, and to enhance the understanding of HONO formation mechanisms by evaluating the influence of key factors on HONO variation. To achieve these objectives, we used a 0-dimensional photochemical model and newly introduced the Artificial Neuron Network (ANN) method.

2 METHODOLOGY

2.1 Measurement

During the KORUS-AQ campaign, ground measurements were conducted at Olympic Park (37.57˚, 127.14˚) in Seoul to get a comprehensive view of air quality (Figure 1). Olympic Park is 145 ha of natural green area located southeast of the city center. The Han river flows northeast of the park, along which the Olympic Expressway extends. The details about measurement will be found in Kim et al., 2019.

HONO was measured by the three institutions using the two techniques: Parallel Plate Diffusion Scrubber coupled with Ion Chromatography (IC) system by Yonsei University and Korea University and Tunable infrared-laser differential absorption spectrometer (TILDAS) with applied quantum cascade (QC) laser by Hankuk University for Foreign Languages. All three measurements showed a reasonable correlation of r = 0.75~0.84. Because optical measurement is free of sampling artifact with high time resolution (Pinto et al., 2014), HONO measurements by the QC-TILDAS were used for further analysis in the present study.

QC-TILDAS was developed by Aerodyne Research Incorporation and is suitable for measuring highly reactive trace gases, especially in the mid-infrared region, because of its high sensitivity, short response time (1 to 10 Hz), and theoretically low detection limit (~0.1 ppb). It determines the mixing ratio of the target trace gas by monitoring its molecular absorption at a certain wavenumber. In this study, we used 1276 cm^{-1} for measuring HONO. HONO data were collected every 1 seconds, and averaged hourly for assimilation with other measurement data. The absorption was then compared with the theoretical spectrum of the HIgh-resolution TRANsmission (HITRAN) database to calculate the mixing ratio of the trace gases. The Tunable Diode Laser Wintel data acquisition program (TDL Wintel) installed in the instrument is designed to perform a frequency scan and acquire the resulting absorption spectrum, and then to analyze the spectrum obtained by the instrument. Dry N_2 gas was injected every 5 minutes to clear out the Multi-Pass Cell (MPC) and stabilize the baseline.

QC-TILDAS requires the management of physical conditions such as the pressure in the absorption chamber,

https://doi.org/10.5194/acp-2019-1012
Preprint. Discussion started: 16 December 2019

Atmospheric Chemistry and Physics Discussions

the temperature of the laser, and the temperature of the detector in order to keep the resolution spectrum stable. Large noise levels were observed in the preliminary measurement data of QC-TILDAS probably due to the difficulty to manage these physical conditions, especially due to the instability of the laser temperature. For this reason, the Kalman filter, which is generally used for estimating and analyzing data from environment with large noise levels, was applied to minimize the noise levels. First, assuming that the spectrum obtained by the non-negative least square method was the reference spectrum, the Kalman filter was applied and then the HONO concentration was sequentially calculated by the non-negative least square method again. All of these calculations were implemented in Python

Equivalent Black Carbon (eBC) was measured using Multi-Angle Absorption Photometer (MAAP, Thermo. Inc) by Korea University of Technology and Education. Particle number concentration was measured using Scanning Mobility Particle Sizer (SMPS, TSI. Inc) by National Institute of Environmental Research (NIER). Along with, were measured reactive trace gases including O_3, NO_x, CO, VOCs, and HCHO, $PM_{2.5}$ mass, and meteorological parameters including temperature, relative humidity (RH), and wind speed (Kim et al., 2019), and mixing layer height (MLH, (Lee et al., 2019). Measurement periods started from 17th May to 10th June 2016, and all data were assimilated as 1 hour averages.

2.2 Model configuration

2.2.1 Framework for 0-D Atmospheric Modeling (F0AM)

Framework for 0-D Atmospheric Modeling (F0AM) was developed by (Wolfe et al., 2016), which was advanced version from the 1-D Chemistry of Atmosphere-Forest Exchange (CAFE). Its prior objective is to simulate the chemical and physical process within the forest canopy, but it is also capable of tracing the change in chemical pollutants in other environments. Due to the intrinsic nature of the model, it may overestimate the influence of the vegetation, but it is suitable for this study because of the campaign period, which are most affected by the biogenic emissions. F0AM is written in MATLAB and provides the option to choose the one of chemical reactions based on Master Chemical Mechanism (MCM), Carbon Bond Mechanism (CB05), Regional Atmospheric Chemistry Mechanism (RACM), and Goddard Earth Observing System – Chemical (GEOS-Chem) mechanism. In this study, we utilized MCMv3.3.1 with the measured chemical and meteorological data sets which were hourly averaged. The dilution factor (k_{dil}) was adjusted and a sensitivity test was conducted by excluding each factor. Finally, we quantified the impact of HONO on OH formation and daily maximum O_3 concentration. The detailed conditions and results are discussed in session 3.3.

2.2.2 Artificial Neural Network (ANN)

The Artificial Neuron Network (ANN) was developed in computer science in the 1940s, but it has only been recent years that successful applications could be possible because of the limitation of computational performance and algorithm problems. Among various disciplines, ANN was integrated into atmospheric sciences to predict the movement of airmass, meteorological change, and pollutant concentration variations (Shrivastava et al., 2012;Ong et al., 2016;Li et al., 2017a;Li et al., 2017b;Nieto et al., 2018;Franceschi et al., 2018;Gardner and Dorling, 1998). ANN applied not only in atmospheric science, but also in quantum chemistry for calculating energy state of HONO (Pradhan and Brown, 2017). In comparison, there is little attempts to understand how the input data are related to output results in ANN, because it is difficult to evaluate the weight of each neural network nodes. Therefore, in this study, we applied the ANN for the first

https://doi.org/10.5194/acp-2019-1012
Preprint. Discussion started: 16 December 2019

Atmospheric Chemistry and Physics Discussions

time to estimate the impact of each input factor to output HONO concentrations and approximately evaluate the weight of each input species.

To easily construct the ANN model, we utilized powerful '*neuralnet*' packages in R (Riedmiller and Rprop, 1994;Anastasiadis et al., 2005). Description for ANN models are written in references, and we changed the stepmax from 10^5 to 10^8 and repetitions from 1 to 3 for making calculation be possible and more accurate. Also, we fix the random number sets using function offered from R for the repeatability of ANN model. To get the integrity of data, we selected the data set from which all input factors are usable. Because the range of the measurement data set is largely different, all data are normalized (x_{nor}) to the range of HONO using Eq. (2), application form of Eq. (1):

$$x_{nor} = \frac{x - minimum(X)}{maximum(X) - minimum(X)} \quad (1)$$

x_{nor} is the normalized value for X using '*min-max scaling*' (Mohamad and Usman, 2013;Patel and Mehta, 2011). Then, x_{nor} was adjusted to the HONO concentration scale following Eq. (2):

$$x_{nor,HONO} = \frac{x - minimum(X)}{maximum(X) - minimum(X)} \times (maximum(HONO) - minimum(HONO)) + minimum(HONO) \quad (2)$$

In a fully-connected artificial neural network (FC-ANN) which has only 1 hidden layer, the output (y) is calculated by the Eq. (3) (Figure 2).

$$y = \phi\left(h_{1,0}w_0^{out} + h_{1,1}w_1^{out} + h_{1,2}w_2^{out} + \cdots + h_{1,j}w_j^{out}\right) = \phi\left(\sum_{m=0}^{j} h_{1,m}w_m^{out}\right) \quad (3)$$

The $h_{1,m}$ indicates the value of m^{th} node in 1st hidden layer, and the w_m^{out} indicates the weight of m^{th} node in a 1st hidden layer to the output. The terms expressed using 0 ($h_{1,0}$, and w_0^{out}) come from 'bias' terms, which were represented as '+1' in the calculation. As similar as the propagation method from 1st hidden layer to output, each node value in a 1st hidden layer can be shown as the result of the activation function which includes the sum of the multiple of input layer variables (x) and weight (w) following Eq. (4):

$$h_{1,m} = \phi\left(x_0 w_0^{h_{1,m}} + x_1 w_1^{h_{1,m}} + x_2 w_2^{h_{1,m}} + \cdots + x_i w_i^{h_{1,m}}\right) = \phi\left(\sum_{n=0}^{i} x_n w_n^{h_{1,m}}\right), \text{ where } 1 \le m \le j \quad (4)$$

In general, the results of the activation function are represented as $\phi(z)$, where z is the sum of multiple input (x, or h) and weights (w). Therefore, z can be written as $\sum_{m=0}^{j} h_m w_m^{out}$ or $\sum_{n=0}^{i} x_n w_n^{h_{1,m}}$, meaning that we can compare the weight of each variable such as w_m^{out} or $w_n^{h_{1,m}}$ because they are linearly coupled, and the result z is proportional to the $\phi(z)$. However, there was a little issue for using the weight directly because the range and sign are different in each weight. Therefore, we employed the softmax function, $\text{softmax}(w_p) = \frac{e^{w_p}}{\sum_{k=1}^{l} e^{w_k}}$, where $1 \le p \le l$. It is widely used for measuring the portion of each variable p, due to its advantage that makes all variables in the range between 0 and 1. By applying this function, we can compare the weight of each variable as Eq. (5) and Eq. (6):

https://doi.org/10.5194/acp-2019-1012
Preprint. Discussion started: 16 December 2019

Atmospheric Chemistry and Physics Discussions

246 weight of $h_{1,j}$ in hidden layer to y in output $(P_y^{h_{1,j}}) = \frac{e^{w_j^{out}}}{\sum_{m=0}^{j} e^{w_m^{out}}}$, (5)

247 weight of x_i in input layer to $h_{1,j}$ in hidden layer $(P_{h_{1,j}}^{x_i}) = \frac{e^{w_i^{h_{1,j}}}}{\sum_{n=0}^{i} e^{w_n^{h_{1,j}}}}$, (6)

248

249 As a result, we can estimate the influence of x_i to the final result (y) using Eq. (7):

250 weight of x_i in input layer to y in output $= 100(\%) \times \sum_{m=1}^{j}(P_{h_m}^{x_i} \times P_y^{h_m})$, (7)

251

252 **3 RESULTS AND DISCUSSION**

253

254 **3.1 Characteristic variation of HONO**

255

256 During the measurement, the average HONO concentration was 0.93 ppbv in the range of 0.07~3.46 ppbv, and
257 the average O_3 concentration was 40.6 ppbv in the range of 0.8~127.8 ppbv (Figure 3). When compared to the previous
258 measurement study, the HONO concentration in this study was lower than other urban sites (0.44~2.80 ppbv) (Table 1),
259 but it is obviously higher than suburban (0.28~0.66 ppbv) or rural (0.16~0.65 ppbv) sites.

260 In the entire experiment, there were 14 days when O_3 concentration exceeded 90 ppbv, close to the 95 %ile of
261 O_3 concentration (91.5 ppbv), which corresponds to the 'Unhealthy for sensitive groups' level of the Comprehensive Air-
262 quality Index (CAI). Thus, 17, 18, 19, 20, 22, 23, 25, 29, and 30 May, and 2, 5, 7, 9, and 10 June were categorized as
263 'high O_3 episodes', and the other 11 days were categorized as 'non-episodes'. O_3 and HONO concentrations were higher
264 in high O_3 episodes than non-episodes: average O_3 and HONO concentrations were 41.0 and 1.05 ppbv in high O_3 episodes,
265 and 40.1 and 0.81 ppbv in non-episodes, respectively. Especially, these differences were evident for the 95 %ile
266 concentration of O_3 and HONO, which were 94.7 and 2.58 ppbv during high O_3 episodes, and 79.7 and 1.91 ppbv for
267 non-episodes, respectively.

268 These High O_3 periods were distinguished by synoptic meteorological conditions: stagnant or transport period
269 in May and blocking period in June (Miyazaki et al., 2019). While the distribution of major chemical species was greatly
270 affected by the local or synoptic circulation of the atmosphere in May, the air mass was relatively homogeneous and aged
271 under domestic influence in June (Kim et al., 2019). It resulted in noticeable difference in chemical and meteorological
272 characteristics between May and June. For example, the daytime temperature was higher by 2.2 ℃ in May than June, and
273 the average CO concentration was higher by 178 ppbv in May than June. The NO_x and VOCs concentrations were also
274 higher in May than June. The mean NO and NO_2 concentrations were 11.1and 30.1 ppbv in May and 6.9 and 25.6 ppbv
275 in June, respectively, leading to higher NO_2/NO in June than May. The sum of Benzene, Toluene, Ethylbenzene, and o-
276 Xylene (BTEX) was 52.5 ppbC in May and 43.6 ppbC in June, on average. At lower precursor levels, however, the
277 daytime concentrations of HCHO and PAN were slightly higher in June than May. Likewise, the 95 %ile HONO
278 concentration at night was higher in June (2.41 ppbv) than May (2.39 ppbv). This result demonstrates that HONO was
279 intimately coupled with photochemical oxidation process during the KORUS-AQ campaign.

280 In general, HONO and O_3 showed an inverse correlation (Figure 4). In the present study, the overall correlation
281 between the two species was good ($r^2 = 0.41$). Interestingly, the nighttime HONO was higher during the high O_3 episodes
282 than other days. Comparing with the high O_3 episodes and non-episodes, average nighttime HONO concentrations (00~05
283 LST) was 1.82 ppbv in high O_3 episodes and 1.20 ppbv in non-episodes. BTEX concentration was higher at nighttime

https://doi.org/10.5194/acp-2019-1012
Preprint. Discussion started: 16 December 2019

Atmospheric Chemistry and Physics Discussions

than daytime on both high O_3 and non-episodes. In comparison, HCHO showed a clear peak in the morning and afternoon, corresponding to the maximum concentration of NO_x and O_3, respectively. It is likely that HONO was photolyzed in the early morning, and the OH produced by HONO photolysis oxidized VOCs that was accumulated at night, generating HCHO. Consequently, O_3 was formed as a final product, which will be discussed in terms of HONO-VOCs-O_3 chain in section 3.2.

NO_x showed a typical diurnal variation in urban areas with a rush hour peak at 8 am and started to increase again at 4 pm shortly after O_3 reached its maximum. In particular, NO_2 remained high during the night, implicitly indicating the possibility of NO_2-HONO interaction at high RH environment if high HONO was observed. While HONO was positively correlated with NO_x, the correlation was better for NO_2 ($r^2 = 0.39$) than NO ($r^2 = 0.22$). HONO is also well correlated with CO due to the common in diurnal variation with higher concentration at nighttime than daytime, in accordance with the change in MLH. $PM_{2.5}$ and eBC showed an inversed pattern in their diurnal variation, albeit not clear. It implies that there was contribution from secondary formation to $PM_{2.5}$, in addition to the influence of local emission, airmass change, and transport.

HONO concentration increased with the increase of RH up to 80 %, where the maximum HONO was observed (Figure 5). When RH was over 80 %, however, HONO concentration decreased. This type of RH dependency has been reported in previous studies, and several hypotheses were suggested (Cui et al., 2018a;Huang et al., 2017;Li et al., 2012). Figure 5 also illustrates that the highest HONO was associated with the top 10 % of NO_x in all RH ranges except for those with RH > 80 %. In Korea, RH = 80 % is the criteria that distinguishes haze and mist. Thus, it can be said that the conversion of HONO from NO_x was most efficient under haze conditions. Under high RH, the active surfaces available for HONO formation would have been scavenged into mist particles. These results are convincing evidence for the active role of NO_x and aerosol surface in the formation of HONO. The detailed homogeneous-heterogeneous HONO formation mechanism will be further discussed in section 3.3.

3.2 O_3 formation through HONO-HO_x-VOCs mechanism under sunlight

As we stated in a previous chapter, HONO concentration was higher during the high O_3 episodes than non-episodes, and it was highlighted at nighttime (Figure 6). It is already known that HONO affects the daily OH budget, so we compared the OH concentration produced from HONO photolysis (R1) between high O_3 episodes and non-episodes. In previous studies, the steady-state HONO mixing ratio ($[HONO]_{ss}$) was calculated using the following Eq. (8) with concentrations of NO ([NO]) and OH ([OH]), a photolysis rate constant of R1 (J_{HONO}), and reaction rate constant of R2 (k_2) and R11 (k_3) (Kleffmann, 2007;Wong et al., 2012).

$$HONO + OH \rightarrow NO + H_2O \quad \text{(R11)}$$

$$[HONO]_{ss} = \frac{k_2[NO][OH]}{J_{HONO}+k_3[OH]}, \quad (8)$$

In this study, the OH mixing ratio was estimated using the measured HONO concentration, assuming that OH is produced only from HONO. The photolysis rate constant of HONO (J_{HONO}) was calculated using Eq. (9), which was developed by (Hayman, 1997), complemented by (Jenkin et al., 1997;Saunders et al., 2003), and incorporated in MCM photolysis calculations (Wolfe et al., 2016).

https://doi.org/10.5194/acp-2019-1012
Preprint. Discussion started: 16 December 2019

Atmospheric Chemistry and Physics Discussions

$$J = l\,(\cos(SZA))^m\, exp(-n\sin(SZA)), \quad (9)$$

The constant l, m, and n are 0.002644, 0.261, and -0.288, respectively. The calculated J_{HONO} is in the range between 0.6×10^{-4} s^{-1} and 0.2×10^{-2} s^{-1} with an average of 0.1×10^{-2} s^{-1}, which is close to those of other measurement references (Wong et al., 2012;Li et al., 2012). Finally, OH mixing ratio was calculated from Eq. (10):

$$[OH] = J_{HONO}([HONO]_{t1} - [HONO]_{t2}), \quad (10)$$

The estimated OH produced by HONO was significantly different between high O_3 episodes and non-episodes. While the averaged OH concentration showed little difference in the afternoon (12:00~18:00 LST) between high O_3 episode (0.24±0.18 pptv) and non-episode (0.22±0.15 pptv), the OH concentration of the early morning (5:00~11:00 LST) was noticeably higher in high O_3 episode (0.41±0.25 pptv) than non-episode (0.27±0.14 pptv). The integrated OH concentration produced by HONO photolysis was also higher in high O_3 episodes ($\int_{early\ morning} OH\ dt$ = 2.87 pptv, $\int_{afternoon} OH\ dt$ = 1.66 pptv) than non-episode ($\int_{early\ morning} OH\ dt$ = 1.92 pptv, $\int_{afternoon} OH\ dt$ = 1.56 pptv). This simple estimation and comparison highlight the role of HONO in OH production.

In addition, F0AM was run with our measurements of HONO, BTEX, and HCHO for the period of June, to quantitatively understand the role of HONO in HONO-HO_x-O_3 chain. In June, there were 5 days of high O_3 episodes and details regarding measurements are stated in chapter 3.1. First, we adjusted the model configuration so that it properly simulated the measured O_3 maximum and diurnal variation, which is a control run (S1) (Figure 7). Then, the model was run with the three scenarios for comparison (Table 2). Without BTEX (S2), the maximum O_3 was decreased by 33.7 ppbv. If HCHO as well as BTEX was not included (S3), the maximum O_3 concentration was lowered as large as 65.8 ppbv. The S4 scenario without HONO reduced O_3 by 50.3 ppbv and shifted the maximum to morning. The result of sensitivity test demonstrates the significant role of HONO in diurnal photochemical cycle.

For control scenario (S1), we estimated the contribution of HONO to HO_x and O_3 concentration by comparing high O_3 episodes with non-episodes in June (Figure 8). The nighttime HONO concentration was higher by 0.04~0.7 ppbv in high O_3 episode than non-episode, promoting the production of HO_x radicals: 0.1~0.2 pptv of OH in early morning and late afternoon and 4.7~15.8 pptv of HO_2 in the late afternoon. Consequently, it resulted in increase in maximum O_3 by about 20 ppbv. The results of F0AM model calculation confirm the role of HONO in HO_x cycle in such that the photolysis of HONO produces OH radical in the early morning, initiating the photochemical reaction involving VOCs and NO_x and facilitating the formation of O_3.

3.3 Insight into HONO formation mechanism

Despite the importance of HONO in photochemistry, detailed HONO formation mechanism is still not clear. It has been proposed that NO, NO_2, and H_2O are intimately linked in HONO formation through physical mechanism as well as chemical reactions. However, it is still difficult to quantitatively determine the contribution of each precursor to HONO formation. Among all reactions, we examined the role of NO, NO_2 and RH in HONO formation through R3, R6, and R7. Their relative importance was estimated simply by correlating HONO concentration with the product of all reactant

https://doi.org/10.5194/acp-2019-1012
Preprint. Discussion started: 16 December 2019

Atmospheric Chemistry and Physics Discussions

concentration as a surrogate of production rate. For all three reactions, the surrogate was positively correlated with HONO, in which the low and high HONO was associated with low (~60 %) and high (60~90 %) RH, respectively. It suggests RH is critical parameter determining HONO concentration under high NO_x environment like Seoul.

Because HONO concentration stayed high at night from 0 am to 5 am (LST), the HONO formation mechanism was investigated under this time zone, considering HONO photolysis, SZA, and MLH. In addition, we distinguished the direct HONO emission ($[HONO]_{emission}$) from the chemical HONO formation ($[HONO]_{formation}$). The direct emission of HONO from the tailpipe of vehicle was estimated as about 0.65 % of total NO_x concentration (Kurtenbach et al., 2001;Liu et al., 2017), which is commonly used in recent studies (Qin et al., 2009;Tong et al., 2015;Cui et al., 2018a). In the present study, $[HONO]_{emission}$ is in the range from 0.02 to 0.53 ppbv with a mean of 0.17 ppbv. $[HONO]_{formation}$ is calculated by subtracting $[HONO]_{emission}$ from measured HONO concentrations. Using this $[HONO]_{formation}$, we calculated the conversion ratio of NO_x ($C_{HONO,NOx}$) to HONO from the following Eq. (11), which was application of suggested equation in previous studies (Alicke et al., 2002;Alicke et al., 2003;Su et al., 2008;Hou et al., 2016).

$$C_{HONO,NO_x} = \frac{[HONO]_{cor,t2}-[HONO]_{cor,t1}}{(t_2-t_1)\times[\overline{NO_x}]} \quad (11)$$

It assumes that all HONO was only converted by NO and NO_2 in the nighttime. The average NO_x to HONO conversion ratio is 0.86×10^{-2} h^{-1}. It is similar to the NO_2 conversion ratio of Shanghai (Cui et al., 2018a), and is in the range of urban and rural areas which were reported in previous studies (Li et al., 2012;Xu et al., 2015;Huang et al., 2017;Wang et al., 2015). As expected, the conversion ratio was increased along with the increase of RH until 80 %, as 1.06×10^{-2} h^{-1} (Figure 9.a). However, the conversion ratio decreased when RH was over 80 %, like the HONO concentration. This phenomenon already reported, and Wojtal et al., suggested that it was caused by the surface loss or particle loss in marine boundary layers, which is in accordance with what we found in the present study discussed in section 3.1 (Liu et al., 2019b;Wojtal et al., 2011).Therefore, the observed HONO is likely to be formed through heterogeneous conversion which is mainly controlled by factors like NO_x, RH, and surface area.

In previous study, BC particles were suggested to serve as catalyst for heterogeneous reactions by providing active sites for H_2O and gaseous species owing to its complex microstructure (Zhang et al., 2008). The mass concentration of eBC is available in this study and showed similar variation with C_{HONO,NO_x} against RH (Figure. 9.b). In urban areas, the count median diameter (CMD) of fresh BC particle is typically found between 50 nm and 80 nm, and the range of CMD is broadened approximately 30 to 120 nm when air mass is affected by a plume from aircraft engine exhaust or wildfire (Petzold et al., 2005;Reddington et al., 2013). Based on number-size distributions obtained from the SMPS measurement, the dry surface area was estimated, assuming that particles with a diameter of 30 nm to 121.9 nm likely represent BC. Similarly to eBC and C_{HONO,NO_x}, the calculated surface area reached the maximum around RH = 80 % (Figure 9.d). In comparison, $PM_{2.5}$ mass concentration was linearly increased with RH (Figure 9.c). In addition, there was no consistent relationship between the total surface areas of particles smaller than 500 nm measured by SMPS and C_{HONO,NO_x}, either.

Finally, we employed an Artificial Neural Network (ANN) method to test sensitivity and quantify the contribution of NO_x, H_2O, and surface area on HONO formation (Figure 2). For model training and validating, we used measurements of NO, NO_2, temperature (°C), RH (%), surface area of the 30~121 nm diameter range, wind speed, MLH, and SZA.

https://doi.org/10.5194/acp-2019-1012
Preprint. Discussion started: 16 December 2019

Atmospheric Chemistry and Physics Discussions

To optimized node numbers in the hidden layer, we constructed the ANN from 8 to 20 of nodes which were in the proper range of other references (Qiu et al., 2018). In addition, the k-fold cross validation method was applied for more appropriate approach, using the number of k = 7. The performance of model was evaluated by the correlation coefficient between the observed HONO ($HONO_{obs}$) and modeled HONO ($HONO_{mod}$). First, the measurement data was divided into seven sets, of which the six subsets were used to train the ANN and the left one was to validate the result of ANN. This process was repeated for all combinations of seven subsets with varying the number of nodes from 8 to 20 and iteration. Lastly, the correlation coefficient was averaged and the node number shown the highest coefficient was selected. Consequently, the seven time of repeated training with 11 nodes resulted in the best correlation coefficient (r = 0.74). For the training sets with 11 nodes, the 6^{th} iteration gave the highest correlation coefficient (r = 0.85).

In this configuration, ANN was employed to test the sensitivity of eight selected variables to HONO concentration. As shown in Figure 10, the total weight of 8 variables was 61.1%. Of these, the weight of four variables including NO, NO_2, RH, and surface area was substantial (> 10 %), in which the weight of NO_x (26.2 %) was evidently higher than that of surface area (11.9 %) or RH (10.6 %). The weight of other meteorology-related variables such as SZA or MLH was relatively low, compare to those of chemical variables. It is probably because they are tightly coupled with day-night cycle. The ANN model result is a convincing evidence for the heterogeneous formation of HONO from NO_x in urban atmosphere, albeit not fully explained by eight variables. There could be other sources than the three reactions considered in this study such as soil emission or removal processes. Nonetheless, this study clearly demonstrates that the ANN model realistically simulates the ambient HONO concentration using the measured variables and highlights that NO_x, surface area, and RH are key factors for HONO formation in Seoul during the early summer.

4 CONCLUSIONS

To identify key mechanisms for high levels of O_3 and $PM_{2.5}$ in Seoul Metropolitan Areas (SMA) and to get solid evidences for implementing policies, the KORUS-AQ (Korea-US Air Quality Study) campaign was conducted during May ~ June 2016. As part of it, O_3 and trace gases including HONO were measured at Olympic Park in Seoul, a key ground site.

HONO was measured using Quantum Cascade Tunable Diode Laser Absorption Spectroscopy (QC-TILDAS) at 1276 cm^{-1} every 1 second, which was averaged for 1 h for subsequent analysis. The theoretical detection limit was better than 0.1 ppbv. For the entire experiment, the HONO concentration ranged from 0.07 ppbv to 3.46 ppbv with the mean of 0.93 ppbv. HONO showed a typical diurnal cycle with the maximum at 4 am, and remained low but above the detection limit during the day. The daily maximum concentration of HONO was different between the high-O_3 episodes and non-episode. The high-O_3 episodes were selected for a total of 14 days based on the daily maximum O_3 of 90 ppbv (Kim et al., 2019). The 95 %tile concentrations of O_3 and HONO were much higher in high O_3 episodes (94.7 ppbv and 2.58 ppbv) than in non-episodes (79.1 ppbv and 1.91 ppbv). Similarly, the concentrations of NO_x, VOCs, and HCHO were higher in high-O_3 periods than non-episodes. It implies that HONO is closely linked to the photochemical oxidation process that produces O_3.

When OH concentration was calculated using J_{HONO} assuming that OH production from HONO photolysis is the only OH source, it was about 50 % higher in the early morning (5~11 am) during high-O_3 episodes (2.87 pptv) compared to non-episodes (1.92 pptv). In addition, the photochemical F0AM model was utilized to simulate diurnal photochemical cycle of HO_x radicals and O_3 using the measurements of HONO and VOCs in June. The nighttime HONO

https://doi.org/10.5194/acp-2019-1012
Preprint. Discussion started: 16 December 2019

Atmospheric Chemistry and Physics Discussions

concentration of 0.3 ppbv that is the difference between the high-O_3 episodes and non-episode lead to the enhancement of OH and HO_2 concentrations in the morning and afternoon, respectively, thereby increasing the maximum O_3 concentration by 20 ppbv.

The HONO concentration was increased with RH until 80 %, which was evident under high NO_x condition (top 10 %). It implies that NO_x is converted to HONO and this process is facilitated by humidity. The conversion ratio of NO_x to HONO was estimated from the measured NO_x and HONO concentrations and the average ratio was 0.86×10^{-2} h^{-1} at night from 0 am to 5 am. The conversion ratio was highest at RH of 70~80 %. Similarly, the surface area of particles between 30 nm and 121.9 nm in diameter and the mass concentration of eBC showed a similar trend for RH, as a surrogate for aerosol surfaces where HONO formation can be catalyzed. Based on this empirical evidence, HONO concentrations were successfully simulated in an Artificial Neural Network model with the eight measurement variables. Of these, NO, NO_2, RH, and surface area were found to be the main factors that have the greatest impact on ambient HONO concentrations. For the best suite of the ANN calculation and the measurement ($r = 0.85$), the weight values of NO_x, RH, and surface area comprised 26.2 %, 10.6 %, and 11.9 %, respectively. This ANN model results demonstrate the heterogeneous formation of HONO in SMA under high NO_x condition. Consequently, ANN approach can be a useful alternative to conventional model for investigating formation mechanisms of atmospheric constituents, which are not unequivocally understood.

5 AUTHOR CONTRIBUTION

All authors participated in ground measurements at Olympic Park in Seoul during the KORUS-AQ campaign. J. Gil, J. Kim, M. Lee, G. Lee, D. Lee measured HONO with difference methods. In particular, TILDAS system was run by J. Kim and G. Lee. J. An established the platform for ground measurement. J. Jung, S. Cho, J. Hong, J. Lee, and R. Long made measurements of NO_x and CO, VOCs, mixing layer height, eBC, and HCHO, respectively. J. Gil and M. Lee were responsible for model simulations and writing the manuscript.

6 ACKNOWLEDGEMENTS

This research was conducted as part of KORUS-AQ project, and study was financially funded by the National Research Foundation of Korea (2017R1A2B4012143). Specially thanks to National Aeronautics and Space Administration and National Institute of Environmental Research for supporting the experiment.

https://doi.org/10.5194/acp-2019-1012
Preprint. Discussion started: 16 December 2019

Atmospheric Chemistry and Physics Discussions

7 TABLES AND FIGURES

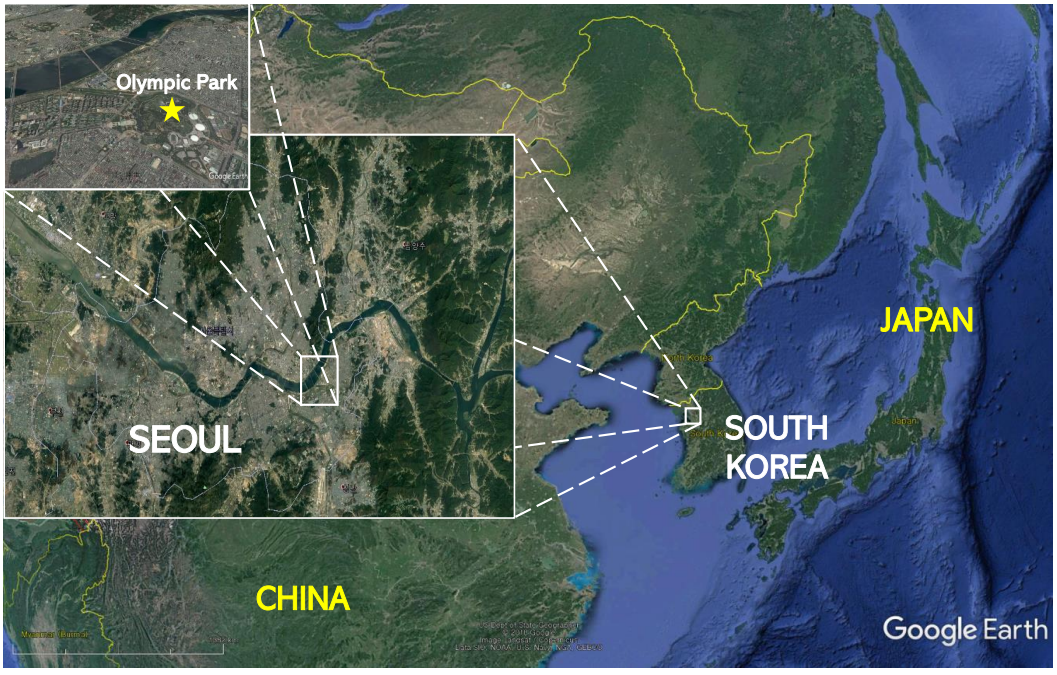

Figure 1. The map shows the location of Olympic Park as a key surface measurement site in Seoul, South Korea. (© Google Earth)

https://doi.org/10.5194/acp-2019-1012
Preprint. Discussion started: 16 December 2019

Atmospheric Chemistry and Physics Discussions

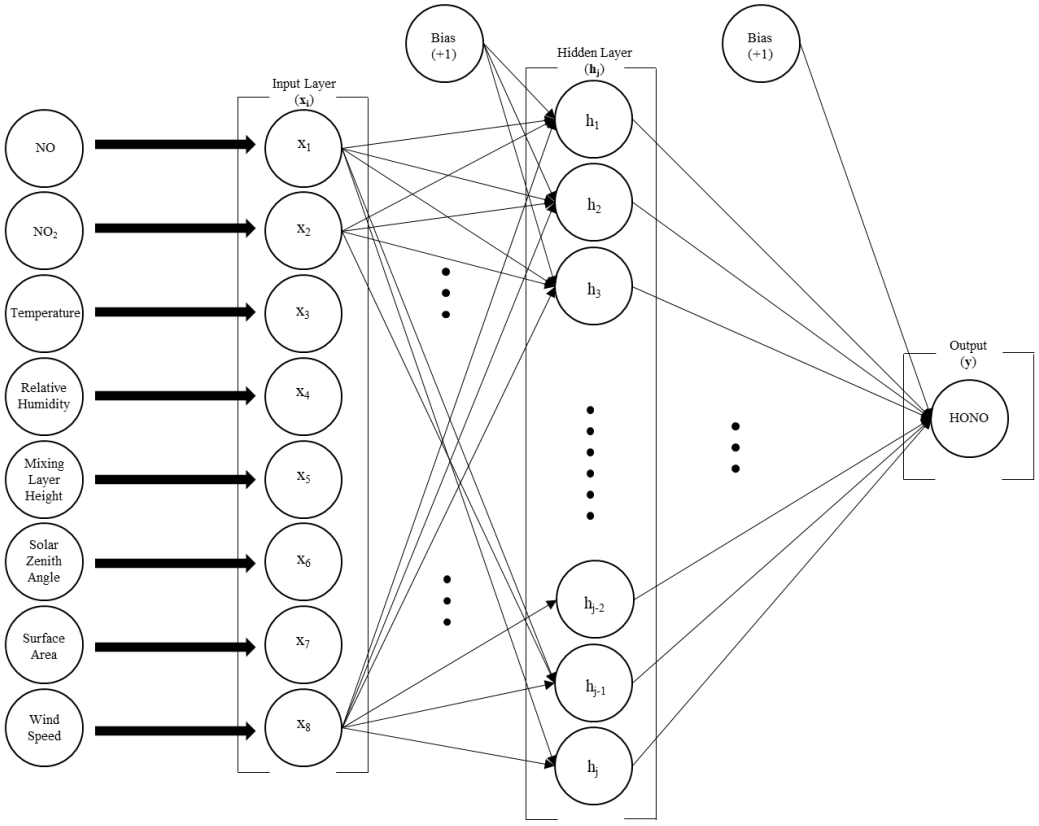

Figure 2. Structure of fully connected artificial neuron network (FC-ANN) model used in this study. In general ANN expression, the equation of output is $\mathbf{y} = \boldsymbol{\phi}(\sum \boldsymbol{xw} + \boldsymbol{b})$. In this study, we express the bias term '$\boldsymbol{b}$' as $\boldsymbol{x_0 w_0}$.

https://doi.org/10.5194/acp-2019-1012
Preprint. Discussion started: 16 December 2019

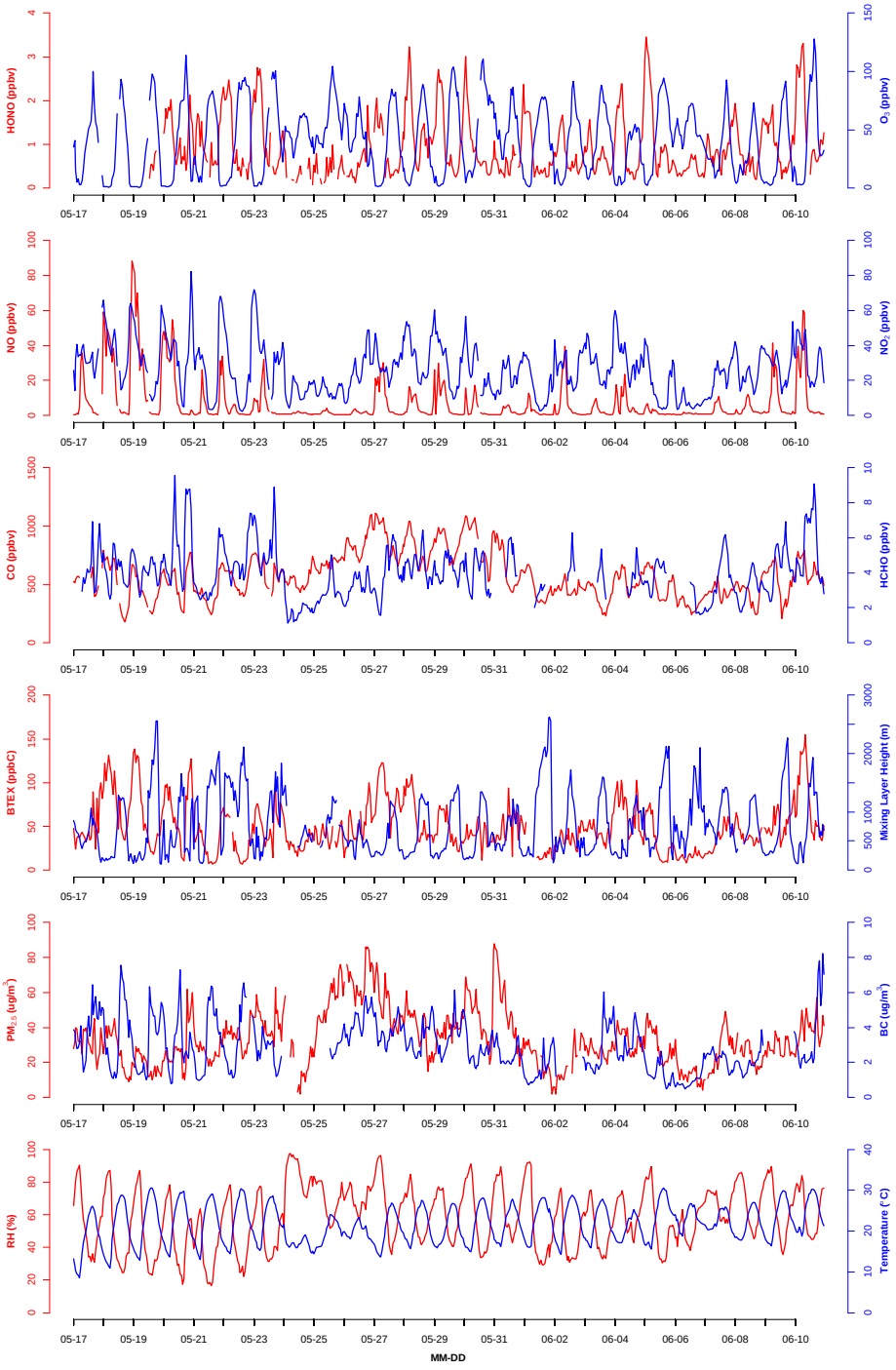

Figure 3. The variation of selected species measured at Olympic park during the KORUS-AQ campaign.

https://doi.org/10.5194/acp-2019-1012
Preprint. Discussion started: 16 December 2019

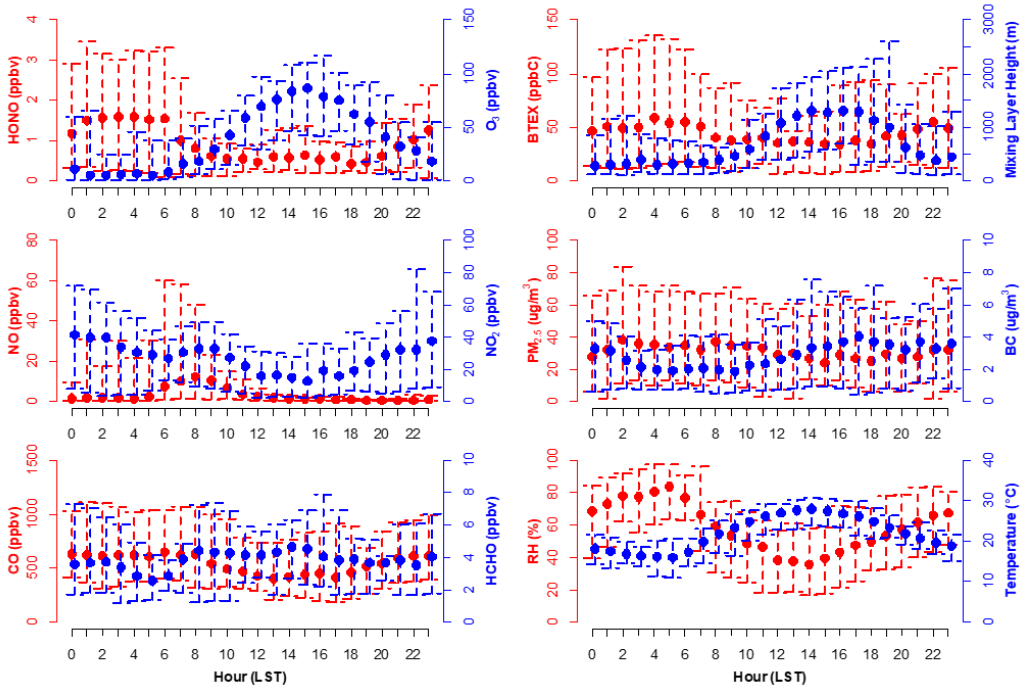

Figure 4. Diurnal variations of selected species measured at Olympic Park during the KORUS-AQ campaign.

https://doi.org/10.5194/acp-2019-1012
Preprint. Discussion started: 16 December 2019

Atmospheric Chemistry and Physics Discussions

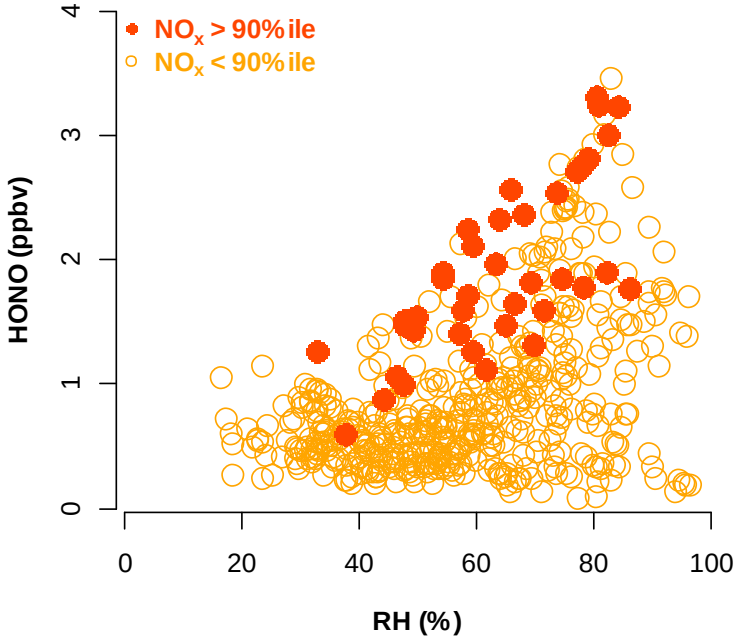

484

485 Figure 5. Correlation between HONO and RH color-coded with NO_x level for entire measurements.

https://doi.org/10.5194/acp-2019-1012
Preprint. Discussion started: 16 December 2019

Atmospheric Chemistry and Physics Discussions

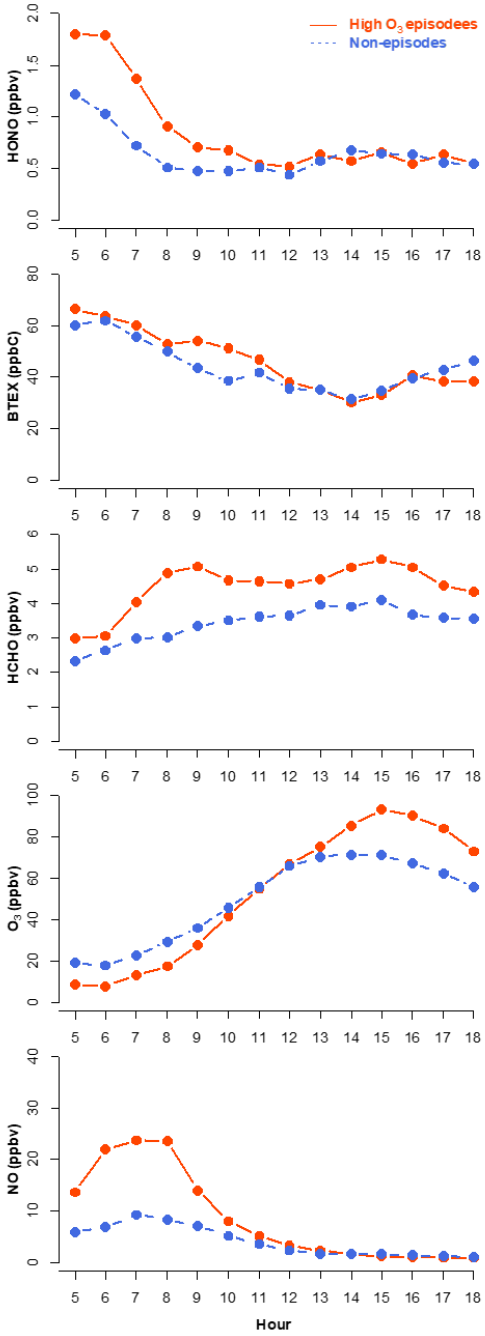

Figure 6. Diurnal variations of HONO, the sum of benzene, toluene, ethylbenzene, and xylene (BTEX), HCHO, O_3, and NO during the high-O_3 episodes and non-episode for the entire experiment.

https://doi.org/10.5194/acp-2019-1012
Preprint. Discussion started: 16 December 2019

Atmospheric Chemistry and Physics Discussions

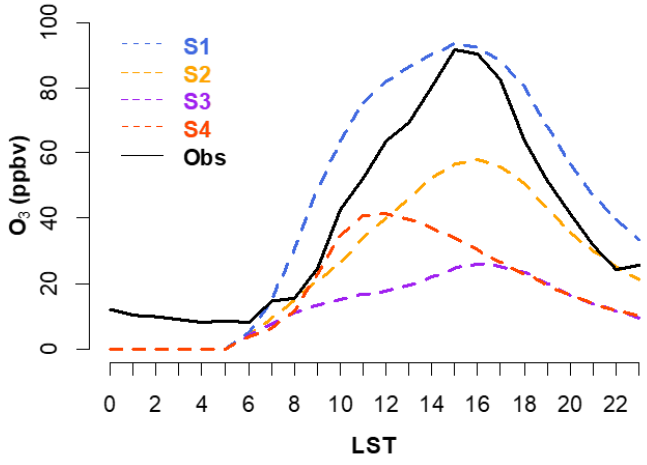

489

490 Figure 7. Diurnal variation of modeled O_3 in case of each scenario

https://doi.org/10.5194/acp-2019-1012
Preprint. Discussion started: 16 December 2019

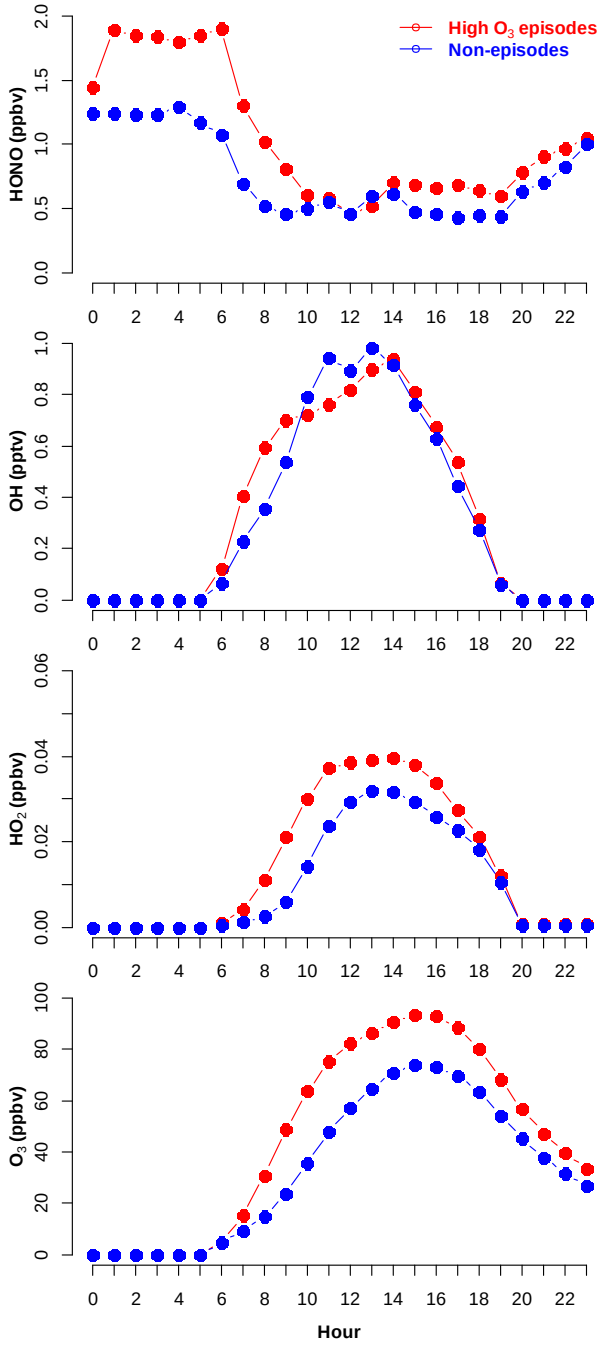

Figure 8: Diurnal variation of observed HONO, and modeled OH, HO_2, and O_3 using measurement data of high O_3 episodes and non-episodes

https://doi.org/10.5194/acp-2019-1012
Preprint. Discussion started: 16 December 2019

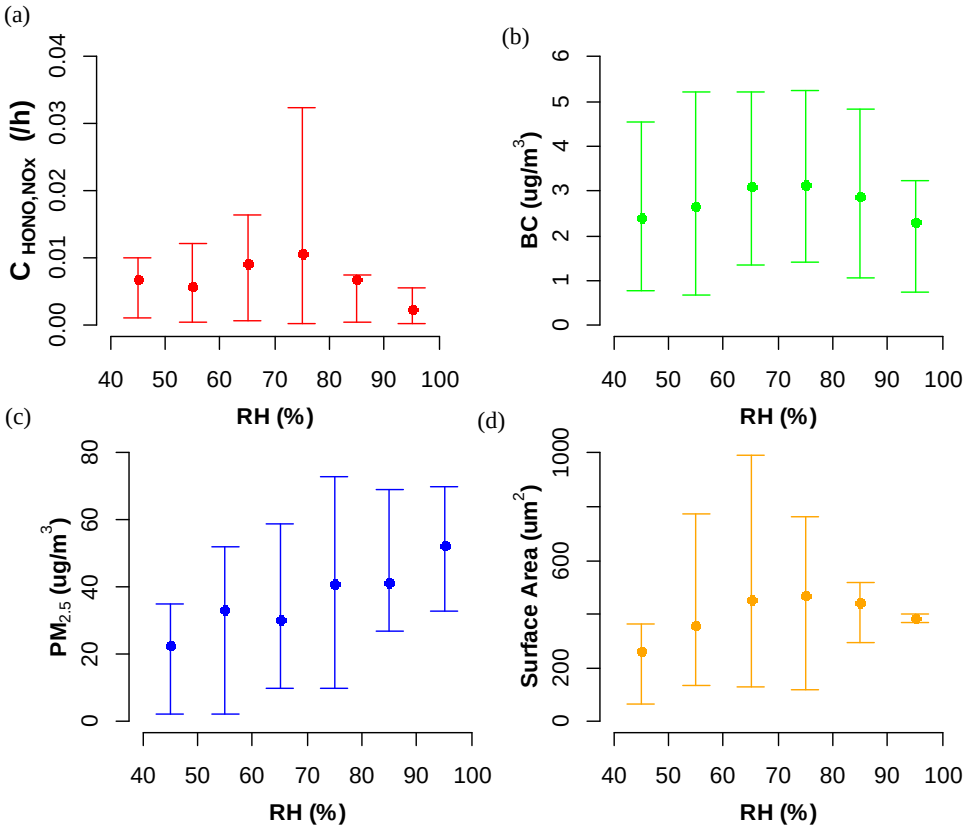

Figure 9. Relationship between (a) conversion ratio of NOx to HONO (see the text), (b) eBC mass concentration, (c) $PM_{2.5}$ mass concentration, (d) surface area of particles between 30 to 120 nm diameter obtained from SMPS measurement against relative humidity (RH). Solid circle represents the mean, and the upper and lower bar stands for Q_1 - 1.5IQR, and Q_3 + 1.5IQR, respectively.

https://doi.org/10.5194/acp-2019-1012
Preprint. Discussion started: 16 December 2019

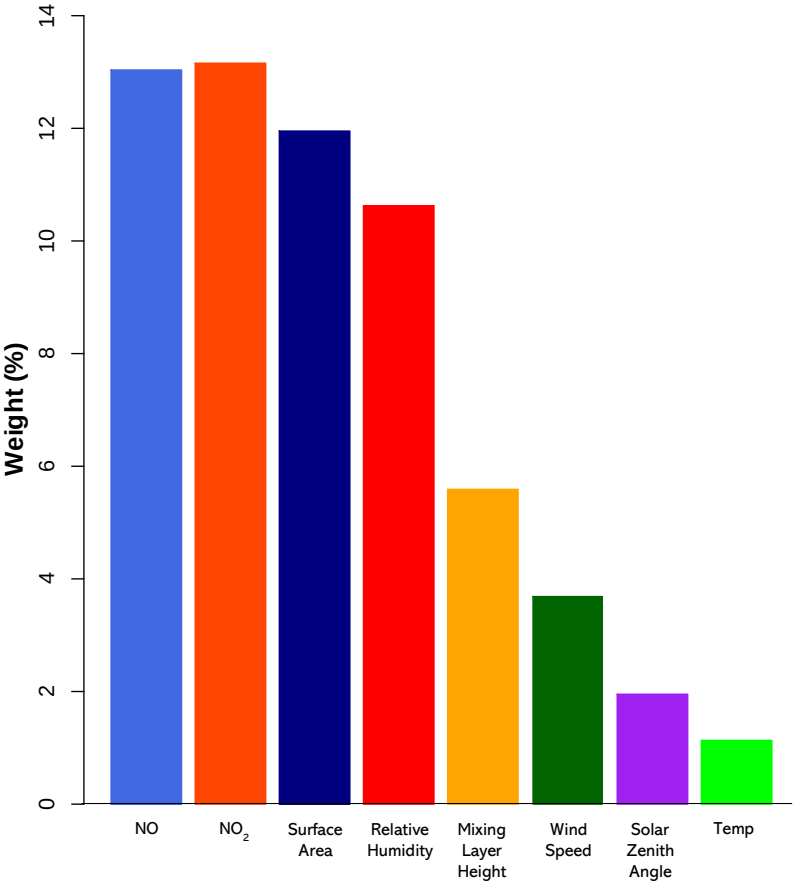

Figure 10. Weight percent of variables indicating their impact on HONO concentration in artificial neural network (ANN) model.

https://doi.org/10.5194/acp-2019-1012
Preprint. Discussion started: 16 December 2019

Atmospheric Chemistry and Physics Discussions

506 Table 1. The summary of HONO measurements from previous studies.

Type	Location	Period	Maen (ppbv)	Method*	Reference
Urban					
	Hebei, China	Jun	2.57	SC-IC	(Xue et al., 2019)
	Shanghai, China	May	2.31	LOPAP	(Cui et al., 2018a)
	Kensington, UK	Jul~Aug	1.05	LOPAP	(Lee et al., 2016)
	Shanghai, China	Oct	1.30	LOPAP	(Bernard et al., 2016)
	Xi'an, China	Jul~Aug	1.12	LOPAP	(Huang et al., 2017)
	Guangzhou, China	Jul	2.80	DOAS	
	Beijing, China (Suburban~Urban)	Dec	0.44~1.34	DOAS/GAC	(Qin et al., 2009)
Suburban					
	Tungchung, HK	Summer	0.66	LOPAP	(Xu et al., 2015)
	Palaiseau, France	Jul	0.28	NitroMAC	(Michoud et al., 2014)
Rural					
	Wangdu, China	Jun~Jul	0.49	LOPAP	(Tan et al., 2018)
	Norfolk coast, UK	Jun~Jul	0.16	LOPAP	(Reed et al., 2016)
	Gyeong-Gi, South Korea	Jun	0.65	PPDS-IC	(Kim et al., 2015)
	Seoul, South Korea	Aug	1.23	LP-DOAS	(Lee et al., 2005)
	Seoul, South Korea	May~Jul	0.36	HEDS	(Song et al., 2009)
This study					
		May~Jun	0.93	QC-TILDAS#	

507 *Full name

508 # HONO was measured using PPDS-IC technique and their mean concentrations were lower than that of TILDAS.

509

510

511 Table 2. F0AM model configuration and four scenarios used in the present study.

k_{dil} : 21600 s^{-1} (6 hr^{-1})	S1	S2	S3	S4
HONO	O	O	O	X
BTEX (only o-xylene)	O	X	X	O
HCHO	O	O	X	O
$*O_{3_{mod}}/O_{3_{obs}}$	1.02	0.63	0.28	0.45

512 * Daily maximum concentration.

513

https://doi.org/10.5194/acp-2019-1012
Preprint. Discussion started: 16 December 2019

Atmospheric Chemistry and Physics Discussions

8 REFERENCS

Alicke, B., Platt, U., and Stutz, J.: Impact of nitrous acid photolysis on the total hydroxyl radical budget during the Limitation of Oxidant Production/Pianura Padana Produzione di Ozono study in Milan, Journal of Geophysical Research: Atmospheres, 107, LOP 9-1-LOP 9-17, 2002.

Alicke, B., Geyer, A., Hofzumahaus, A., Holland, F., Konrad, S., Pätz, H., Schäfer, J., Stutz, J., Volz-Thomas, A., and Platt, U.: OH formation by HONO photolysis during the BERLIOZ experiment, Journal of Geophysical Research: Atmospheres, 108, PHO 3-1-PHO 3-17, 2003.

Allegrini, I., De Santis, F., Di Palo, V., Febo, A., Perrino, C., Possanzini, M., and Liberti, A.: Annular denuder method for sampling reactive gases and aerosols in the atmosphere, Science of the Total Environment, 67, 1-16, 1987.

Anastasiadis, A. D., Magoulas, G. D., and Vrahatis, M. N.: New globally convergent training scheme based on the resilient propagation algorithm, Neurocomputing, 64, 253-270, 2005.

Appel, B., Winer, A., Tokiwa, Y., and Biermann, H.: Comparison of atmospheric nitrous acid measurements by annular denuder and differential optical absorption systems, Atmospheric Environment. Part A. General Topics, 24, 611-616, 1990.

Aumont, B., Chervier, F., and Laval, S.: Contribution of HONO sources to the NOx/HOx/O3 chemistry in the polluted boundary layer, Atmospheric Environment, 37, 487-498, 2003.

Bao, F., Li, M., Zhang, Y., Chen, C., and Zhao, J.: Photochemical Aging of Beijing Urban PM2. 5: HONO Production, Environmental science & technology, 52, 6309-6316, 2018.

Bari, A., Ferraro, V., Wilson, L. R., Luttinger, D., and Husain, L.: Measurements of gaseous HONO, HNO3, SO2, HCl, NH3, particulate sulfate and PM2. 5 in New York, NY, Atmospheric Environment, 37, 2825-2835, 2003.

Barsotti, F., Bartels-Rausch, T., De Laurentiis, E., Ammann, M., Brigante, M., Mailhot, G., Maurino, V., Minero, C., and Vione, D.: Photochemical formation of nitrite and nitrous acid (HONO) upon irradiation of nitrophenols in aqueous solution and in viscous secondary organic aerosol proxy, Environmental science & technology, 51, 7486-7495, 2017.

Bejan, I., El Aal, Y. A., Barnes, I., Benter, T., Bohn, B., Wiesen, P., and Kleffmann, J.: The photolysis of ortho-nitrophenols: a new gas phase source of HONO, Physical Chemistry Chemical Physics, 8, 2028-2035, 2006.

Bernard, F., Cazaunau, M., Grosselin, B., Zhou, B., Zheng, J., Liang, P., Zhang, Y., Ye, X., Daële, V., and Mu, Y.: Measurements of nitrous acid (HONO) in urban area of Shanghai, China, Environmental Science and Pollution Research, 23, 5818-5829, 2016.

Bhattarai, H. R., Virkajärvi, P., Yli-Pirilä, P., and Maljanen, M.: Emissions of atmospherically important nitrous acid (HONO) gas from northern grassland soil increases in the presence of nitrite (NO2−), Agriculture, ecosystems & environment, 256, 194-199, 2018.

Brandenburger, U., Brauers, T., Dorn, H.-P., Hausmann, M., and Ehhalt, D. H.: In-situ measurements of tropospheric hydroxyl radicals by folded long-path laser absorption during the field campaign POPCORN, in: Atmospheric Measurements during POPCORN—Characterisation of the Photochemistry over a Rural Area, Springer, 181-204, 1998.

Cui, L., Li, R., Zhang, Y., Meng, Y., Fu, H., and Chen, J.: An observational study of nitrous acid (HONO) in Shanghai, China: The aerosol impact on HONO formation during the haze episodes, Science of The Total Environment, 630, 1057-1070, 2018a.

Cui, L., Li, R., Fu, H., Li, Q., Zhang, L., George, C., and Chen, J.: Formation features of nitrous acid in the offshore area of the East China Sea, Science of The Total Environment, 682, 138-150, 2019.

Cui, X., Yu, R., Chen, W., Zhang, Z., Pang, T., Sun, P., Xia, H., Wu, B., and Dong, F.: Development of a Quantum Cascade Laser-based Sensor for Environmental HONO Monitoring in the mid-Infrared at 8 μm, Journal of Lightwave Technology, 2018b.

Ermel, M., Behrendt, T., Oswald, R., Derstroff, B., Wu, D., Hohlmann, S., Stönner, C., Pommerening-Röser, A., Könneke, M., and Williams, J.: Hydroxylamine released by nitrifying microorganisms is a precursor for HONO emission from drying soils, Scientific reports, 8, 1877, 2018.

Febo, A., Perrino, C., and Allegrini, I.: Measurement of nitrous acid in Milan, Italy, by DOAS and diffusion denuders, Atmospheric Environment, 30, 3599-3609, 1996.

Ferm, M., and Sjödin, A.: A sodium carbonate coated denuder for determination of nitrous acid in the atmosphere, Atmospheric Environment (1967), 19, 979-983, 1985.

Finlayson-Pitts, B., Wingen, L., Sumner, A., Syomin, D., and Ramazan, K.: The heterogeneous hydrolysis of NO 2 in laboratory systems and in outdoor and indoor atmospheres: An integrated mechanism, Physical Chemistry Chemical Physics, 5, 223-242, 2003.

Fortner, E. C., Zhao, J., and Zhang, R.: Development of ion drift-chemical ionization mass spectrometry, Analytical chemistry, 76, 5436-5440, 2004.

Franceschi, F., Cobo, M., and Figueredo, M.: Discovering relationships and forecasting PM10 and PM2. 5 concentrations in Bogotá, Colombia, using Artificial Neural Networks, Principal Component Analysis, and k-means clustering, Atmospheric Pollution Research, 2018.

Fu, X., Wang, T., Zhang, L., Li, Q., Wang, Z., Xia, M., Yun, H., Wang, W., Yu, C., and Yue, D.: The significant contribution

https://doi.org/10.5194/acp-2019-1012
Preprint. Discussion started: 16 December 2019

Atmospheric Chemistry and Physics Discussions

572 of HONO to secondary pollutants during a severe winter pollution event in southern China, Atmospheric Chemistry and
573 Physics, 19, 1-14, 2019.
574 Garcia-Nieto, D., Benavent, N., and Saiz-Lopez, A.: Measurements of atmospheric HONO vertical distribution and
575 temporal evolution in Madrid (Spain) using the MAX-DOAS technique, Science of The Total Environment, 643, 957-
576 966, 2018.
577 Gardner, M. W., and Dorling, S.: Artificial neural networks (the multilayer perceptron)—a review of applications in the
578 atmospheric sciences, Atmospheric environment, 32, 2627-2636, 1998.
579 Gu, J., Zhang, Y., Zeng, L., and Wen, M.: Evaluation of the Performance of a Gas and Aerosol Collector (GAC), Research
580 of Environmental Sciences, 22, 16-22, 2009.
581 Han, C., Yang, W., Yang, H., and Xue, X.: Enhanced photochemical conversion of NO2 to HONO on humic acids in the
582 presence of benzophenone, Environmental pollution, 231, 979-986, 2017.
583 Hayman, G.: Effects of pollution control on UV exposure, AEA Technology Final Report prepared for the Department of
584 Health and Contract, 121, 6377, 1997.
585 Heland, J., Kleffmann, J., Kurtenbach, R., and Wiesen, P.: A new instrument to measure gaseous nitrous acid (HONO) in
586 the atmosphere, Environmental Science & Technology, 35, 3207-3212, 2001.
587 Hendrick, F., Müller, J.-F., Clémer, K., Wang, P., Mazière, M. D., Fayt, C., Gielen, C., Hermans, C., Ma, J., and Pinardi,
588 G.: Four years of ground-based MAX-DOAS observations of HONO and NO 2 in the Beijing area, Atmospheric
589 Chemistry and Physics, 14, 765-781, 2014.
590 Hou, S., Tong, S., Ge, M., and An, J.: Comparison of atmospheric nitrous acid during severe haze and clean periods in
591 Beijing, China, Atmospheric Environment, 124, 199-206, 2016.
592 Huang, R.-J., Yang, L., Cao, J., Wang, Q., Tie, X., Ho, K.-F., Shen, Z., Zhang, R., Li, G., and Zhu, C.: Concentration and
593 sources of atmospheric nitrous acid (HONO) at an urban site in Western China, Science of The Total Environment, 593,
594 165-172, 2017.
595 Jenkin, M. E., Saunders, S. M., and Pilling, M. J.: The tropospheric degradation of volatile organic compounds: a protocol
596 for mechanism development, Atmospheric Environment, 31, 81-104, 1997.
597 Keuken, M. P., Schoonebeek, C. A., van Wensveen-Louter, A., and Slanina, J.: Simultaneous sampling of NH3, HNO3,
598 HC1, SO2 and H2O2 in ambient air by a wet annular denuder system, Atmospheric Environment (1967), 22, 2541-2548,
599 1988.
600 Kim, H., Choi, W.-C., Rhee, H.-J., Suh, I., Lee, M., Blake, D. R., Kim, S., Jung, J., Lee, G., and Kim, D.-S.:
601 Meteorological and Chemical Factors Controlling Ozone Formation in Seoul during MAPS-Seoul 2015, Aerosol and Air
602 Quality Research, 18, 2274-2286, 2018a.
603 Kim, S., Kim, S.-Y., Lee, M., Shim, H., Wolfe, G., Guenther, A. B., He, A., Hong, Y., and Han, J.: Impact of isoprene and
604 HONO chemistry on ozone and OVOC formation in a semirural South Korean forest, Atmospheric Chemistry and Physics,
605 15, 4357-4371, 2015.
606 Kim, S., Sanchez, D., Wang, M., Seco, R., Jeong, D., Hughes, S., Barletta, B., Blake, D. R., Jung, J., and Kim, D.: OH
607 reactivity in urban and suburban regions in Seoul, South Korea–an East Asian megacity in a rapid transition, Faraday
608 discussions, 189, 231-251, 2016.
609 Kim, S., Jeong, D., Sanchez, D., Wang, M., Seco, R., Blake, D., Meinardi, S., Barletta, B., Hughes, S., and Jung, J.: The
610 Controlling Factors of Photochemical Ozone Production in Seoul, South Korea, Aerosol and Air Quality Research, 18,
611 2253-2261, 2018b
612 Kim, H., Lee, M., Gil, J., Jung, J., Long, W. R., Lee, G., Kim, D., Cho, S., Ahn, J., Hong, J., Park, M.: Overview and
613 charactersitics of air quality in Seoul Metropolitan Area during the KORUS-AQ campaign, Elementa: Science of the
614 Anthropocene, *be submitted*, 2019.
615 Kleffmann, J., Lörzer, J., Wiesen, P., Kern, C., Trick, S., Volkamer, R., Rodenas, M., and Wirtz, K.: Intercomparison of
616 the DOAS and LOPAP techniques for the detection of nitrous acid (HONO), Atmospheric Environment, 40, 3640-3652,
617 2006.
618 Kleffmann, J.: Daytime sources of nitrous acid (HONO) in the atmospheric boundary layer, ChemPhysChem, 8, 1137-
619 1144, 2007.
620 Komazaki, Y., Shimizu, H., and Tanaka, S.: A new measurement method for nitrogen oxides in the air using an annular
621 diffusion scrubber coated with titanium dioxide, Atmospheric Environment, 33, 4363-4371, 1999.
622 Kotamarthi, V., Gaffney, J., Marley, N., and Doskey, P.: Heterogeneous NOx chemistry in the polluted PBL, Atmospheric
623 Environment, 35, 4489-4498, 2001.
624 Koutrakis, P., Wolfson, J. M., Slater, J. L., Brauer, M., Spengler, J. D., Stevens, R. K., and Stone, C. L.: Evaluation of an
625 annular denuder/filter pack system to collect acidic aerosols and gases, Environmental science & technology, 22, 1463-
626 1468, 1988.
627 Kurtenbach, R., Becker, K., Gomes, J., Kleffmann, J., Lörzer, J., Spittler, M., Wiesen, P., Ackermann, R., Geyer, A., and
628 Platt, U.: Investigations of emissions and heterogeneous formation of HONO in a road traffic tunnel, Atmospheric
629 Environment, 35, 3385-3394, 2001.
630 Lee, B. H., Wood, E. C., Zahniser, M. S., McManus, J. B., Nelson, D. D., Herndon, S. C., Santoni, G., Wofsy, S. C., and

https://doi.org/10.5194/acp-2019-1012
Preprint. Discussion started: 16 December 2019

Atmospheric Chemistry and Physics Discussions

631 Munger, J. W.: Simultaneous measurements of atmospheric HONO and NO 2 via absorption spectroscopy using tunable
632 mid-infrared continuous-wave quantum cascade lasers, Applied Physics B, 102, 417-423, 2011.
633 Lee, C., Kim, Y. J., Hong, S.-B., Lee, H., Jung, J., Choi, Y.-J., Park, J., Kim, K.-H., Lee, J.-H., and Chun, K.-J.:
634 Measurement of atmospheric formaldehyde and monoaromatic hydrocarbons using differential optical absorption
635 spectroscopy during winter and summer intensive periods in Seoul, Korea, Water, Air, and Soil Pollution, 166, 181-195,
636 2005.
637 Lee, J., Whalley, L., Heard, D., Stone, D., Dunmore, R., Hamilton, J., Young, D., Allan, J., Laufs, S., and Kleffmann, J.:
638 Detailed budget analysis of HONO in central London reveals a missing daytime source, Atmospheric Chemistry and
639 Physics, 16, 2747-2764, 2016.
640 Lee, J., Hong, J.-W., Lee, K., Hong, J., Velasco, E., Lim, Y. J., Lee, J. B., Nam, K., and Park, J.: Ceilometer Monitoring
641 of Boundary-Layer Height and Its Application in Evaluating the Dilution Effect on Air Pollution, Boundary-Layer
642 Meteorology, 1-21, 2019.
643 Levy, M., Zhang, R., Zheng, J., Zhang, A. L., Xu, W., Gomez-Hernandez, M., Wang, Y., and Olaguer, E.: Measurements
644 of nitrous acid (HONO) using ion drift-chemical ionization mass spectrometry during the 2009 SHARP field campaign,
645 Atmospheric environment, 94, 231-240, 2014.
646 Li, L., Duan, Z., Li, H., Zhu, C., Henkelman, G., Francisco, J. S., and Zeng, X. C.: Formation of HONO from the NH3-
647 promoted hydrolysis of NO2 dimers in the atmosphere, Proceedings of the National Academy of Sciences, 115, 7236-
648 7241, 2018.
649 Li, S., Matthews, J., and Sinha, A.: Atmospheric hydroxyl radical production from electronically excited NO2 and H2O,
650 Science, 319, 1657-1660, 2008.
651 Li, T., Shen, H., Yuan, Q., Zhang, X., and Zhang, L.: Estimating Ground-Level PM2. 5 by Fusing Satellite and Station
652 Observations: A Geo-Intelligent Deep Learning Approach, Geophysical Research Letters, 44, 2017a.
653 Li, X., Brauers, T., Häseler, R., Bohn, B., Fuchs, H., Hofzumahaus, A., Holland, F., Lou, S., Lu, K., and Rohrer, F.:
654 Exploring the atmospheric chemistry of nitrous acid (HONO) at a rural site in Southern China, Atmospheric Chemistry
655 and Physics, 12, 1497-1513, 2012.
656 Li, X., Peng, L., Yao, X., Cui, S., Hu, Y., You, C., and Chi, T.: Long short-term memory neural network for air pollutant
657 concentration predictions: Method development and evaluation, Environmental Pollution, 231, 997-1004, 2017b.
658 Li, Z., Liu, Y., Lin, Y., Gautam, S., Kuo, H.-C., Tsai, C.-J., Yeh, H., Huang, W., Li, S.-W., and Wu, G.-J.: Development of
659 an automated system (PPWD/PILS) for studying PM2. 5 water-soluble ions and precursor gases: Field measurements in
660 two cities, Taiwan, Aerosol Air Qual. Res, 17, 426-443, 2017c.
661 Liang, Y., Zha, Q., Wang, W., Cui, L., Lui, K. H., Ho, K. F., Wang, Z., Lee, S.-c., and Wang, T.: Revisiting nitrous acid
662 (HONO) emission from on-road vehicles: A tunnel study with a mixed fleet, Journal of the Air & Waste Management
663 Association, 67, 797-805, 2017.
664 Liao, W., Hecobian, A., Mastromarino, J., and Tan, D.: Development of a photo-fragmentation/laser-induced fluorescence
665 measurement of atmospheric nitrous acid, Atmospheric Environment, 40, 17-26, 2006.
666 Liu, Y., Lu, K., Ma, Y., Yang, X., Zhang, W., Wu, Y., Peng, J., Shuai, S., Hu, M., and Zhang, Y.: Direct emission of nitrous
667 acid (HONO) from gasoline cars in China determined by vehicle chassis dynamometer experiments, Atmospheric
668 Environment, 169, 89-96, 2017.
669 Liu, Y., Lu, K., Li, X., Dong, H., Tan, Z., Wang, H., Zou, Q., Wu, Y., Zeng, L., and Hu, M.: A Comprehensive Model Test
670 of the HONO Sources Constrained to Field Measurements at Rural North China Plain, Environmental science &
671 technology, 2019a.
672 Liu, Y., Nie, W., Xu, Z., Wang, T., Wang, R., Li, Y., Wang, L., Chi, X., and Ding, A.: Contributions of different sources to
673 nitrous acid (HONO) at the SORPES station in eastern China: results from one-year continuous observation, Atmos.
674 Chem. Phys. Discuss., 2019, 1-47, 10.5194/acp-2019-219, 2019b.
675 Lu, X., Wang, Y., Li, J., Shen, L., and Fung, J. C.: Evidence of heterogeneous HONO formation from aerosols and the
676 regional photochemical impact of this HONO source, Environmental Research Letters, 13, 114002, 2018.
677 Makkonen, U., Virkkula, A., Mäntykenttä, J., Hakola, H., Keronen, P., Vakkari, V., and Aalto, P.: Semi-continuous gas
678 and inorganic aerosol measurements at a Finnish urban site: comparisons with filters, nitrogen in aerosol and gas phases,
679 and aerosol acidity, Atmospheric Chemistry and Physics, 12, 5617-5631, 2012.
680 Meusel, H., Tamm, A., Kuhn, U., Wu, D., Leifke, A. L., Fiedler, S., Ruckteschler, N., Yordanova, P., Lang-Yona, N., and
681 Pöhlker, M.: Emission of nitrous acid from soil and biological soil crusts represents an important source of HONO in the
682 remote atmosphere in Cyprus, Atmospheric Chemistry and Physics, 18, 799-813, 2018.
683 Michoud, V., Colomb, A., Borbon, A., Miet, K., Beekmann, M., Camredon, M., Aumont, B., Perrier, S., Zapf, P., and
684 Siour, G.: Study of the unknown HONO daytime source at a European suburban site during the MEGAPOLI summer and
685 winter field campaigns, Atmospheric Chemistry and Physics, 14, 2805-2822, 2014.
686 Miyazaki, K., Sekiya, T., Fu, D., Bowman, K., Kulawik, S., Sudo, K., Walker, T., Kanaya, Y., Takigawa, M., and Ogochi,
687 K.: Balance of Emission and Dynamical Controls on Ozone During the Korea-United States Air Quality Campaign From
688 Multiconstituent Satellite Data Assimilation, Journal of Geophysical Research: Atmospheres, 124, 387-413, 2019.
689 Mohamad, I. B., and Usman, D.: Standardization and its effects on K-means clustering algorithm, Research Journal of

https://doi.org/10.5194/acp-2019-1012
Preprint. Discussion started: 16 December 2019

Atmospheric Chemistry and Physics Discussions

690 Applied Sciences, Engineering and Technology, 6, 3299-3303, 2013.
691 Nieto, P. G., Lasheras, F. S., García-Gonzalo, E., and de Cos Juez, F.: PM 10 concentration forecasting in the metropolitan
692 area of Oviedo (Northern Spain) using models based on SVM, MLP, VARMA and ARIMA: a case study, Science of the
693 Total Environment, 621, 753-761, 2018.
694 O'Keefe, A., and Deacon, D. A.: Cavity ring-down optical spectrometer for absorption measurements using pulsed laser
695 sources, Review of Scientific Instruments, 59, 2544-2551, 1988.
696 Ong, B. T., Sugiura, K., and Zettsu, K.: Dynamically pre-trained deep recurrent neural networks using environmental
697 monitoring data for predicting PM2. 5, Neural Computing and Applications, 27, 1553-1566, 2016.
698 Park, M.-S.: Overview of Meteorological Surface Variables and Boundary-Layer Structures in the Seoul Metropolitan
699 Area during the MAPS-Seoul Campaign, Aerosol and Air Quality Research, 18, 2157-2172, 2018.
700 Patel, V. R., and Mehta, R. G.: Impact of outlier removal and normalization approach in modified k-means clustering
701 algorithm, International Journal of Computer Science Issues (IJCSI), 8, 331, 2011.
702 Perner, D., and Platt, U.: Detection of nitrous acid in the atmosphere by differential optical absorption, Geophysical
703 Research Letters, 6, 917-920, 1979.
704 Petzold, A., Gysel, M., Vancassel, X., Hitzenberger, R., Puxbaum, H., Vrochticky, S., Weingartner, E., Baltensperger, U.,
705 and Mirabel, P.: On the effects of organic matter and sulphur-containing compounds on the CCN activation of combustion
706 particles, Atmospheric Chemistry and Physics, 5, 3187-3203, 2005.
707 Pinto, J., Dibb, J., Lee, B., Rappenglück, B., Wood, E., Levy, M., Zhang, R. Y., Lefer, B., Ren, X. R., and Stutz, J.:
708 Intercomparison of field measurements of nitrous acid (HONO) during the SHARP campaign, Journal of Geophysical
709 Research: Atmospheres, 119, 5583-5601, 2014.
710 Pitts, B. F., and Pitts, J.: Chemistry of the upper and lower atmosphere: Theory, experiments and applications, Academic,
711 US, 2000.
712 Plass-Dülmer, C., Brauers, T., and Rudolph, J.: POPCORN: A field study of photochemistry in north-eastern Germany,
713 in: Atmospheric Measurements during POPCORN—Characterisation of the Photochemistry over a Rural Area, Springer,
714 5-31, 1998.
715 Pradhan, E., and Brown, A.: A ground state potential energy surface for HONO based on a neural network with
716 exponential fitting functions, Physical Chemistry Chemical Physics, 19, 22272-22281, 2017.
717 Qin, M., Xie, P., Su, H., Gu, J., Peng, F., Li, S., Zeng, L., Liu, J., Liu, W., and Zhang, Y.: An observational study of the
718 HONO–NO2 coupling at an urban site in Guangzhou City, South China, Atmospheric Environment, 43, 5731-5742, 2009.
719 Qiu, S., Chen, B., Wang, R., Zhu, Z., Wang, Y., and Qiu, X.: Atmospheric dispersion prediction and source estimation of
720 hazardous gas using artificial neural network, particle swarm optimization and expectation maximization, Atmospheric
721 Environment, 178, 158-163, 2018.
722 Reddington, C. L., McMeeking, G., Mann, G. W., Coe, H., Frontoso, M. G., Liu, D., Flynn, M., Spracklen, D. V., and
723 Carslaw, K. S.: The mass and number size distributions of black carbon aerosol over Europe, Atmospheric Chemistry and
724 Physics, 13, 4917-4939, 2013.
725 Reed, C., Brumby, C. A., Crilley, L. R., Kramer, L. J., Bloss, W. J., Seakins, P. W., Lee, J. D., and Carpenter, L. J.: HONO
726 measurement by differential photolysis, Atmospheric Measurement Techniques, 2483-2495, 2016.
727 Riedmiller, M., and Rprop, I.: Rprop-description and implementation details, 1994.
728 Roberts, J. M., Veres, P., Warneke, C., Neuman, J., Washenfelder, R., Brown, S., Baasandorj, M., Burkholder, J., Burling,
729 I., and Johnson, T. J.: Measurement of HONO, HNCO, and other inorganic acids by negative-ion proton-transfer
730 chemical-ionization mass spectrometry (NI-PT-CIMS): Application to biomass burning emissions, Atmospheric
731 Measurement Techniques, 3, 981, 2010.
732 Rohrer, F., Bohn, B., Brauers, T., Brüning, D., Johnen, F.-J., Wahner, A., and Kleffmann, J.: Characterisation of the
733 photolytic HONO-source in the atmosphere simulation chamber SAPHIR, Atmospheric Chemistry and Physics, 5, 2189-
734 2201, 2005.
735 Romer, P. S., Duffey, K. C., Wooldridge, P. J., Allen, H. M., Ayres, B. R., Brown, S. S., Brune, W. H., Crounse, J. D.,
736 Gouw, J. d., and Draper, D. C.: The lifetime of nitrogen oxides in an isoprene-dominated forest, Atmospheric Chemistry
737 and Physics, 16, 7623-7637, 2016.
738 Ryan, R. G., Rhodes, S., Tully, M., Wilson, S., Jones, N., Frieß, U., and Schofield, R.: Daytime HONO, NO 2 and aerosol
739 distributions from MAX-DOAS observations in Melbourne, Atmospheric Chemistry and Physics, 18, 13969-13985, 2018.
740 Ryu, Y.-H., Baik, J.-J., Kwak, K.-H., Kim, S., and Moon, N.: Impacts of urban land-surface forcing on ozone air quality
741 in the Seoul metropolitan area, Atmospheric Chemistry and Physics, 13, 2177-2194, 2013.
742 Saunders, S. M., Jenkin, M. E., Derwent, R., and Pilling, M.: Protocol for the development of the Master Chemical
743 Mechanism, MCM v3 (Part A): tropospheric degradation of non-aromatic volatile organic compounds, Atmospheric
744 Chemistry and Physics, 3, 161-180, 2003.
745 Scherer, J., Paul, J., O'keefe, A., and Saykally, R.: Cavity ringdown laser absorption spectroscopy: history, development,
746 and application to pulsed molecular beams, Chemical reviews, 97, 25-52, 1997.
747 Shrivastava, G., Karmakar, S., Kowar, M. K., and Guhathakurta, P.: Application of artificial neural networks in weather
748 forecasting: a comprehensive literature review, International Journal of Computer Applications, 51, 2012.

https://doi.org/10.5194/acp-2019-1012
Preprint. Discussion started: 16 December 2019

Atmospheric Chemistry and Physics Discussions

Simon, P. K., Dasgupta, P. K., and Vecera, Z.: Wet effluent denuder coupled liquid/ion chromatography systems, Analytical Chemistry, 63, 1237-1242, 1991.
Simon, P. K., and Dasgupta, P. K.: Wet effluent denuder coupled liquid/ion chromatography systems: annular and parallel plate denuders, Analytical Chemistry, 65, 1134-1139, 1993.
Simon, P. K., and Dasgupta, P. K.: Continuous automated measurement of gaseous nitrous and nitric acids and particulate nitrite and nitrate, Environmental science & technology, 29, 1534-1541, 1995.
Song, C. H., Park, M. E., Lee, E. J., Lee, J. H., Lee, B. K., Lee, D. S., Kim, J., Han, J. S., Moon, K. J., and Kondo, Y.: Possible particulate nitrite formation and its atmospheric implications inferred from the observations in Seoul, Korea, Atmospheric Environment, 43, 2168-2173, 2009.
Spataro, F., Ianniello, A., Salvatori, R., Nardino, M., Esposito, G., and Montagnoli, M.: Sources of atmospheric nitrous acid (HONO) in the European High Arctic, Rendiconti Lincei, 28, 25-33, 2017.
Stieger, B., Spindler, G., Fahlbusch, B., Müller, K., Grüner, A., Poulain, L., Thöni, L., Seitler, E., Wallasch, M., and Herrmann, H.: Measurements of PM 10 ions and trace gases with the online system MARGA at the research station Melpitz in Germany–A five-year study, Journal of Atmospheric Chemistry, 75, 33-70, 2018.
Stutz, J., Oh, H.-J., Whitlow, S. I., Anderson, C., Dibb, J. E., Flynn, J. H., Rappenglück, B., and Lefer, B.: Simultaneous DOAS and mist-chamber IC measurements of HONO in Houston, TX, Atmospheric Environment, 44, 4090-4098, 2010.
Su, H., Cheng, Y. F., Cheng, P., Zhang, Y. H., Dong, S., Zeng, L. M., Wang, X., Slanina, J., Shao, M., and Wiedensohler, A.: Observation of nighttime nitrous acid (HONO) formation at a non-urban site during PRIDE-PRD2004 in China, Atmospheric Environment, 42, 6219-6232, 2008.
Su, H., Cheng, Y., Oswald, R., Behrendt, T., Trebs, I., Meixner, F. X., Andreae, M. O., Cheng, P., Zhang, Y., and Pöschl, U.: Soil nitrite as a source of atmospheric HONO and OH radicals, Science, 1207687, 2011.
Sun, R., Hu, W., and Duan, Z.: Prediction of nitrogen solubility in pure water and aqueous NaCl solutions up to high temperature, pressure, and ionic strength, Journal of solution chemistry, 30, 561-573, 2001.
Takeuchi, M., Li, J., Morris, K. J., and Dasgupta, P. K.: Membrane-based parallel plate denuder for the collection and removal of soluble atmospheric gases, Analytical chemistry, 76, 1204-1210, 2004.
Tan, Z., Lu, K., Dong, H., Hu, M., Li, X., Liu, Y., Lu, S., Shao, M., Su, R., and Wang, H.: Explicit diagnosis of the local ozone production rate and the ozone-NOx-VOC sensitivities, Science Bulletin, 63, 1067-1076, 2018.
Tong, S., Hou, S., Zhang, Y., Chu, B., Liu, Y., He, H., Zhao, P., and Ge, M.: Comparisons of measured nitrous acid (HONO) concentrations in a pollution period at urban and suburban Beijing, in autumn of 2014, Science China Chemistry, 58, 1393-1402, 2015.
Tong, S., Hou, S., Zhang, Y., Chu, B., Liu, Y., He, H., Zhao, P., and Ge, M.: Exploring the nitrous acid (HONO) formation mechanism in winter Beijing: direct emissions and heterogeneous production in urban and suburban areas, Faraday discussions, 189, 213-230, 2016.
Tsai, C., Spolaor, M., Colosimo, S. F., Pikelnaya, O., Cheung, R., Williams, E., Gilman, J. B., Lerner, B. M., Zamora, R. J., and Warneke, C.: Nitrous acid formation in a snow-free wintertime polluted rural area, Atmospheric Chemistry and Physics, 18, 1977-1996, 2018.
Wang, G., Zhang, R., Gomez, M. E., Yang, L., Zamora, M. L., Hu, M., Lin, Y., Peng, J., Guo, S., and Meng, J.: Persistent sulfate formation from London Fog to Chinese haze, Proceedings of the National Academy of Sciences, 113, 13630-13635, 2016.
Wang, J., Zhang, X., Guo, J., Wang, Z., and Zhang, M.: Observation of nitrous acid (HONO) in Beijing, China: Seasonal variation, nocturnal formation and daytime budget, Science of the Total Environment, 587, 350-359, 2017.
Wang, L., and Zhang, J.: Detection of nitrous acid by cavity ring-down spectroscopy, Environmental science & technology, 34, 4221-4227, 2000.
Wang, L., Wen, L., Xu, C., Chen, J., Wang, X., Yang, L., Wang, W., Yang, X., Sui, X., and Yao, L.: HONO and its potential source particulate nitrite at an urban site in North China during the cold season, Science of the Total Environment, 538, 93-101, 2015.
Wen, L., Chen, T., Zheng, P., Wu, L., Wang, X., Mellouki, A., Xue, L., and Wang, W.: Nitrous acid in marine boundary layer over eastern Bohai Sea, China: Characteristics, sources, and implications, Science of the Total Environment, 2019.
Wheeler, M. D., Newman, S. M., Orr-Ewing, A. J., and Ashfold, M. N.: Cavity ring-down spectroscopy, Journal of the Chemical Society, Faraday Transactions, 94, 337-351, 1998.
Winer, A., and Biermann, H.: Long pathlength differential optical absorption spectroscopy (DOAS) measurements of gaseous HONO, NO 2 and HCNO in the California South Coast Air Basin, Research on Chemical Intermediates, 20, 423-445, 1994.
Wojtal, P., Halla, J., and McLaren, R.: Pseudo steady states of HONO measured in the nocturnal marine boundary layer: a conceptual model for HONO formation on aqueous surfaces, Atmospheric Chemistry and Physics, 11, 3243-3261, 2011.
Wolfe, G. M., Marvin, M. R., Roberts, S. J., Travis, K. R., and Liao, J.: The Framework for 0-D Atmospheric Modeling (F0AM) v3. 1, Geoscientific Model Development, 9, 3309, 2016.
Wong, K., Tsai, C., Lefer, B., Haman, C., Grossberg, N., Brune, W., Ren, X., Luke, W., and Stutz, J.: Daytime HONO vertical gradients during SHARP 2009 in Houston, TX, Atmospheric Chemistry and Physics, 12, 635-652, 2012.

https://doi.org/10.5194/acp-2019-1012
Preprint. Discussion started: 16 December 2019

Atmospheric Chemistry and Physics Discussions

808 Wu, D., Horn, M. A., Behrendt, T., Müller, S., Li, J., Cole, J. A., Xie, B., Ju, X., Li, G., and Ermel, M.: Soil HONO
809 emissions at high moisture content are driven by microbial nitrate reduction to nitrite: tackling the HONO puzzle, The
810 ISME journal, 1, 2019.
811 Xing, L., Wu, J., Elser, M., Tong, S., Liu, S., Li, X., Liu, L., Cao, J., Zhou, J., and El-Haddad, I.: Wintertime secondary
812 organic aerosol formation in Beijing–Tianjin–Hebei (BTH): contributions of HONO sources and heterogeneous reactions,
813 Atmospheric Chemistry and Physics, 19, 2343-2359, 2019.
814 Xu, Z., Wang, T., Wu, J., Xue, L., Chan, J., Zha, Q., Zhou, S., Louie, P. K., and Luk, C. W.: Nitrous acid (HONO) in a
815 polluted subtropical atmosphere: Seasonal variability, direct vehicle emissions and heterogeneous production at ground
816 surface, Atmospheric environment, 106, 100-109, 2015.
817 Xue, C., Ye, C., Ma, Z., Liu, P., Zhang, Y., Zhang, C., Tang, K., Zhang, W., Zhao, X., and Wang, Y.: Development of
818 stripping coil-ion chromatograph method and intercomparison with CEAS and LOPAP to measure atmospheric HONO,
819 Science of the Total Environment, 646, 187-195, 2019.
820 Yang, W., Han, C., Yang, H., and Xue, X.: Significant HONO formation by the photolysis of nitrates in the presence of
821 humic acids, Environmental pollution, 243, 679-686, 2018.
822 Ye, C., Zhang, N., Gao, H., and Zhou, X.: Photolysis of Particulate Nitrate as a Source of HONO and NO x, Environmental
823 science & technology, 51, 6849-6856, 2017.
824 Zhang, B., and Tao, F.-M.: Direct homogeneous nucleation of NO2, H2O, and NH3 for the production of ammonium
825 nitrate particles and HONO gas, Chemical Physics Letters, 489, 143-147, 2010.
826 Zhang, J., An, J., Qu, Y., Liu, X., and Chen, Y.: Impacts of potential HONO sources on the concentrations of oxidants and
827 secondary organic aerosols in the Beijing-Tianjin-Hebei region of China, Science of the Total Environment, 647, 836-
828 852, 2019a.
829 Zhang, J., Chen, J., Xue, C., Chen, H., Zhang, Q., Liu, X., Mu, Y., Guo, Y., Wang, D., and Chen, Y.: Impacts of six
830 potential HONO sources on HOx budgets and SOA formation during a wintertime heavy haze period in the North China
831 Plain, Science of The Total Environment, 681, 110-123, 2019b.
832 Zhang, R., Khalizov, A. F., Pagels, J., Zhang, D., Xue, H., and McMurry, P. H.: Variability in morphology, hygroscopicity,
833 and optical properties of soot aerosols during atmospheric processing, Proceedings of the National Academy of Sciences,
834 105, 10291-10296, 2008.
835 Zhang, W., Tong, S., Ge, M., An, J., Shi, Z., Hou, S., Xia, K., Qu, Y., Zhang, H., and Chu, B.: Variations and sources of
836 nitrous acid (HONO) during a severe pollution episode in Beijing in winter 2016, Science of The Total Environment, 648,
837 253-262, 2019c.

838

839